

ÉCOLE DE TECHNOLOGIE SUPÉRIEURE
UNIVERSITÉ DU QUÉBEC

THESIS PRESENTED TO
ÉCOLE DE TECHNOLOGIE SUPÉRIEURE

IN PARTIAL FULFILLMENT OF THE REQUIREMENTS FOR
A MASTER'S DEGREE IN MECHANICAL ENGINEERING
M.Eng.

BY
Hassan RADVAR-ESFAHLAN

GEOMETRICAL INSPECTION OF FLEXIBLE PARTS USING
INTRINSIC GEOMETRY

MONTREAL, JULY 14 2010

© Copyright 2010 reserved by Hassan RADVAR-ESFAHLAN

THIS THESIS HAS BEEN EVALUATED
BY THE FOLLOWING BOARD OF EXAMINERS

Mr. Souhail-Antoine Tahan, Ph.D., Thesis Supervisor
Département de génie mécanique à l'École de technologie supérieure

Mr. Jean-François Châtelain, Ph.D., Thesis Co-supervisor
Département de génie mécanique à l'École de technologie supérieure

Mr. Roland Maranzana, Doctorate, President of the Board of Examiners
Département de génie de la production automatisée à l'École de technologie supérieure

Mr. Jean-François Lalonde, Member of Thesis Committee
Bombardier Aéronautique

THIS THESIS HAS BEEN PRESENTED AND DEFENDED
BEFORE A BOARD OF EXAMINERS AND PUBLIC
JULY 14, 2010
AT ÉCOLE DE TECHNOLOGIE SUPÉRIEURE

*To my dear parents, my wife, and
Yashar*

*"All that is in the world is love
And knowledge is nothing but gossip..."*

*« Eşq imiş hər nə var aləmdə
Elm bir qilüqal imiş ancaq ... »
Məhəmməd Füzuli (1483 – 1556).*

INSPECTION GÉOMÉTRIQUE DES PIÈCES FLEXIBLES EN UTILISANT LA GÉOMÉTRIE INTRINSÈQUE

Hassan, RADVAR-ESFAHLAN

RÉSUMÉ

Le problème du tolérancement des pièces mécaniques est décisif pour l'industrie de pointe. Ses incidences économiques sont importantes pour le secteur manufacturier qui subit des transformations profondes imposées par la globalisation des marchés et l'évolution constante des technologies (CAO, CMM, 3D Scanner, etc.). Il est admis aujourd'hui que l'optimisation des performances des produits requiert la prise en compte des variations inhérentes aux processus de fabrication, d'où le contrôle de la qualité à travers le processus de développement et de fabrication. Dans le cas des composantes dites 'flexibles' (ou non rigides), par exemple des pièces mécanique à paroi minces comme le revêtement d'un avion ou d'une auto, l'usage industriel actuel est limité encore à l'utilisation de gabarit de conformité, relativement coûteux, qui contraignent la géométrie de la pièce à un état qui reflète l'assemblage. Par la suite, des mesures par contact directe ou par scanner sont effectuées. C'est ainsi l'industrie élimine l'effet des déformations dues à la flexibilité de la pièce pour tenter de détecter les défauts dus au procédé de fabrication.

Le projet proposé a pour objectif de faciliter les opérations d'inspection dimensionnelle et géométrique des composantes flexibles à partir d'un nuage de points, et ce, sans recours à un gabarit ou des opérations secondaires de conformation. Plus spécifiquement, nous visons le développement d'une méthodologie qui permettra de localiser et de quantifier les défauts de profil dans le cas des coques minces typique des industries aérospatiales et automobiles.

Pour arriver à cet objectif, nous mettons en œuvre une idée que nous appelons *Numerical Inspection Fixture*. Nous utilisons les distances géodésiques pour détecter la similarité intrinsèque entre une pièce à l'état libre qui inclus les effets de gravité, des contraintes internes et des défauts de fabrication, et la même pièce telle que définie nominalement par un modèle CAO. Ce mémoire développe le fondement théorique de cette méthode et les algorithmes qu'y sont reliés. Nous employons une approche, déjà employé dans le domaine de l'imagerie médicale, pour identifier les distances géodésiques minimales (géométrie métrique), les statistiques (*Multidimensional Scaling* - MDS) pour analyser les similarités et dissimilarités entre deux objets, ainsi que la méthode d'éléments finis (FE) pour aboutir à une approche générale et original pour l'inspection de pièces géométriques non rigides. Deux méthodes y sont proposées avec des validations numériques.

Mots-clés: Inspection géométrique; pièces flexibles; géométrie intrinsèque; distance géodésique; fast marching method; multidimensional scaling.

GEOMETRICAL INSPECTION OF FLEXIBLE PARTS USING INTRINSIC GEOMETRY

Hassan, RADVAR-ESFAHLAN

ABSTRACT

The tolerancing of mechanical parts is one of the major problems in modern industry. Its economic consequences are important to the manufacturing sector which sustains major transformations imposed by market globalization and technology evolution (CAD, CMM, 3D Scanners, etc...). Today, we know that product performance optimization requires a consideration of the inherent variations in manufacturing processes, hence quality control throughout the development process and manufacturing. Currently, the geometric inspection of *flexible* (or *nonrigid*) mechanical parts, such as thin-walled skins of airplane or car bodies is still limited to the use of relatively expensive special *inspection fixtures*, which simulate the use state, applying the same constraints that reflect assembly information. Subsequently, contact measuring or scanning is performed. Simulating this use state means that, deformation effects due to flexibility are eliminated. In this way, defects in the manufacturing process are detectable.

The goal of this thesis is to facilitate the dimensional and geometrical inspection of flexible components from a point cloud without using a jig or secondary conformation operation. More specifically, we aim to develop a methodology to localize and quantify the profile defects in the case of thin shells which are typical to the aerospace and automotive industries.

To this end, we implemented an idea that we call *Numerical Inspection Fixtures*. We use geodesic distances to detect the intrinsic similarities between a part in a free state which includes the effects of gravity, internal constraints and manufacturing defects, and the same part as nominally defined by a CAD model. This thesis develops the theoretical foundation of the proposed methods and related algorithms. We used an approach already used in medical image processing to identify minimum geodesic distance and statistics (Multidimensional Scaling) to analyze the similarities and dissimilarities between two objects, as well as the finite element method to reach a general approach for the inspection of nonrigid parts. Two methods are proposed with numerical validations.

Keywords: Geometric inspection; compliant part; intrinsic geometry; geodesic distance; fast marching method; multidimensional scaling.

TABLE OF CONTENTS

| | Page |
|--|------|
| INTRODUCTION | 12 |
| CHAPTER 1 REVIEW OF PREVIOUS RESEARCH | 15 |
| 1.1 Geometric inspection of flexible parts | 15 |
| 1.2 Rigid and nonrigid surface registration | 17 |
| CHAPTER 2 THEORETICAL FOUNDATIONS | 20 |
| 2.1 Metric spaces | 20 |
| 2.2 Point clouds techniques | 22 |
| 2.2.1 Smoothing of noisy data | 22 |
| 2.2.2 Point cloud sampling | 22 |
| 2.2.3 Fast marching method | 24 |
| 2.3 Isometric embedding | 29 |
| 2.4 Generalized multidimensional scaling | 32 |
| CHAPTER 3 NONRIGID GEOMETRIC INSPECTION | 36 |
| 3.1 Geometry of flexible parts | 36 |
| 3.2 Identification of geometrical deviation | 39 |
| 3.3 New definition for maximum geometric deviation | 40 |
| 3.4 Numerical inspection fixture | 42 |
| 3.5 Generalized numerical inspection fixture | 45 |
| CHAPTER 4 RESULTS | 47 |
| 4.1 Geometric inspection in absence of spring-back | 48 |
| 4.2 Inspection results with GNIF | 51 |
| CONCLUSION | 53 |
| Comparison of methods | 53 |
| Limitations of GNIF | 54 |
| Contributions | 54 |
| RECOMMENDATIONS | 57 |
| ANNEX I PUBLICATIONS | 59 |
| ANNEX II SMACOF algorithm | 60 |
| ANNEX III Hausdorff distance algorithm | 62 |
| ANNEX IV GLOSSARY | 64 |
| REFERENCES | 65 |

LIST OF TABLES

| | Page |
|---------|--|
| Table 1 | Numerical fixture verification48 |
| Table 2 | Numerical fixture verification50 |
| Table 3 | Numerical fixture verification50 |
| Table 4 | GNIF verification.....52 |

LIST OF FIGURES

| | | Page |
|------------|--|------|
| Figure 01 | Laser scanning | 12 |
| Figure 02 | Registration process..... | 12 |
| Figure 03 | Inspection fixture | 13 |
| Figure 2.1 | Shortest paths computed by Dijkstra's algorithm..... | 24 |
| Figure 2.2 | Calculation of crossing time at (x, y) for expanding front $F > 0$ | 25 |
| Figure 2.3 | Setup for boundary value formulation..... | 26 |
| Figure 2.4 | Quadratic equation is satisfied by both n and $-n$ | 28 |
| Figure 2.5 | Comparison between FMM and Dijkstra's algorithm..... | 29 |
| Figure 2.6 | Difference between intrinsic and extrinsic similarity..... | 30 |
| Figure 2.7 | Applying the SMACOF algorithm to the first case study..... | 32 |
| Figure 2.8 | Simplified representation of similarity measure..... | 35 |
| Figure 3.1 | Indication and interpretation of ISO 10579..... | 37 |
| Figure 3.2 | Effect of spring-back during geometrical inspection..... | 38 |
| Figure 3.3 | Classification of rigidity of parts..... | 39 |
| Figure 3.4 | Measured point vs. FEM analysis and CAD data..... | 40 |
| Figure 3.5 | Actual and conventional geometric deviation..... | 42 |
| Figure 3.6 | Dedicated inspection fixture for outer panel..... | 43 |

| | | |
|------------|---|----|
| Figure 3.7 | Details of inspection fixture..... | 43 |
| Figure 3.8 | Inspection process flowchart. | 44 |
| Figure 3.9 | Inspection process flowchart using GNIF. | 46 |
| Figure 4.1 | First case study. | 49 |
| Figure 4.2 | Second case study. | 49 |
| Figure 4.3 | Similarity measure between CAD models..... | 50 |
| Figure 4.4 | Third case study..... | 51 |

LIST OF ACRONYMS

| | |
|--------|--|
| 3D | Three-dimensional |
| ASME | American society of mechanical engineers |
| CAD | Computer aided design |
| CAI | Computer aided inspection |
| CAM | Computer aided manufacturing |
| CF | Canonical form |
| CMM | Coordinate measuring machine |
| FPS | Farthest point sampling |
| FEM | Finite element method |
| FMM | Fast marching method |
| GH | Gromov-Hausdorff |
| GNIF | Generalized numerical inspection fixture |
| H | Hausdorff |
| ICP | Iterative closest point |
| IDI | Iterative displacement inspection |
| ISO | International organization for standardization |
| MDS | Multidimensional scaling |
| NURBS | Non-uniform rational B-spline surface |
| SDT | Small displacement torsor |
| SMACOF | Scaling by majorizing a complicated function |

LIST OF NOTATIONS

| | |
|----------------|--|
| y'_i | image of x_i , $x_i \in X$ in Y |
| σ | stress |
| (X, d_X) | metric space where d is a metric on X |
| $\ \dots\ _2$ | Euclidean (or L_2) norm |
| d_{GH} | distance Gromov-Hausdorff |
| d_H | distance Hausdorff |
| $dis f$ | distortion of the map f |
| D_X | symmetric matrix of pairwise geodesic distances with $a_{ii} = 0$. (For n points, it requires $\frac{n(n-1)}{2}$ calculations) |
| $d_X(a, b)$ | distance between a pair of points |
| n | front propagation direction |
| \mathbb{R}^m | m -dimensional Euclidean space |
| $T(Y_M)$ | triangular mesh of Y_M |
| t_i | triangle index |
| X | surface |
| Y_M | space Y sampled by M points |

INTRODUCTION

It is clear that product quality control is essential to company survival in a competitive market. In general, the use of *computer-aided inspection* (CAI) is found to be less well-developed than either that of computer-aided design (CAD) or computer-aided manufacture (CAM). With CAI, raw data from a 3D scanner or CMM can be compared to the original CAD design to generate impressive inspection reports. Topographical color maps highlight deviations between the actual part and the design model, clearly indicating tolerance conditions with far more clarity than traditional CMM (coordinate measuring machine) reports.



Figure 01 Laser scanning

(Turbine blade, taken from Laser Design Inc.)¹



Figure 02 Registration process

(Taken from Laser Design Inc.)¹

Coordinate system *Registration* is required since measured data (point clouds) and the CAD model are not in the same coordinate system. For nonrigid materials, *Inspection Fixtures* are widely used to hold and support the parts for the simulation of use state. Typical examples of such parts are: sheet metal panels, windshields, etc. Generally, for the geometric inspection of such flexible parts, *inspection fixtures*, in combination with coordinate measuring systems, (CMM) are used.

¹ <http://www.laserdesign.com>

The aim of this thesis is to develop a general procedure to eliminate the use of inspection fixtures. Three-dimensional optical digitizing systems are suitable for the measurement of large-sized flexible parts because they allow non-contact measurement and are able to deliver, in a relatively short time, large clouds of points that are representative of object surfaces.

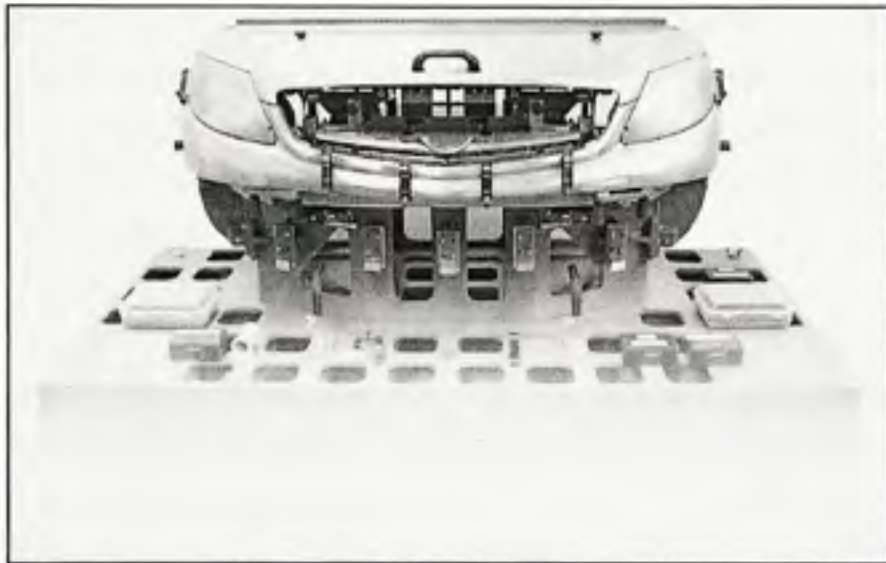


Figure 03 Inspection fixture
(Daimler AG)²

The part is setup on a portable 3D optical digitizing system which is installed in a production line regardless of datum shown in engineering drawings. Due to weight, and of course supports, part deformations occur. An identification method must be defined in order to extract geometrical deviations due to manufacturing defects only. The geometry of flexible parts may vary according to their own weight and the location of supports, so it is essential to detail the ideas around the geometry and inspection of flexible parts.

² <http://www.daimler.com/>

In many cases, it is possible to associate specific products, materials, and manufacturing processes with particular types of seeable surface defects. For instance, injection-moulded components may tend to present undesired sink. Similarly, cutting, grinding, and polishing operations may produce characteristic surface markings, including an altered texture and excessive burrs due to tool wear or the inclusion of foreign abrasive materials. It is important to appreciate that in each case, in addition to possible surface discoloration, these defects tend to induce a deviation in the component's surface shape away from its nominal form. The nature of this deviation, or this type of expected defect, is often somewhat predictable. If, in addition, a causal mechanism can be identified, then a quantitative analysis of such defects may be used as a basis for automatic process control. These surface defects can not only be recognized with *machine vision* technologies, but can also be classified with *pattern recognition* methods. This thesis does not speak to these methods.

The remainder of this thesis presents a theory and method for the geometric inspection of nonrigid parts. Chapter 1 gives a comprehensive literature review of the necessary fields. Chapter 2 gives theoretical foundations in metric and discrete geometry, as well as fast marching methods and multidimensional scaling. In Chapter 3, material is compiled and we present a methodology to measure the geometric deviation of nonrigid bodies. Chapter 4 gives verification to these methods and sample problems.

CHAPTER 1

REVIEW OF PREVIOUS RESEARCH

1.1 Geometric inspection of flexible parts

Traditional tolerance analysis methods, such as *Root Sum Square method* and *Monte Carlo simulation* (Creveling (1997)), are not applicable to compliant parts such as sheet metal assemblies because of possible part deformations during the assembly process. Over the past years, different methods have been presented to predict dimensional variation on flexible parts, especially on sheet metal assemblies. Most of the methods are based on the *Finite Element Method*. Liu and Hu (1997) presented a model to analyze the effect of component deviations and assembly spring-back on assembly variation by applying linear mechanics and statistics. Using FEM, they constructed a sensitivity matrix for compliant parts of complex shapes. The sensitivity matrix established a linear relationship between the incoming part deviation and the output assembly deviation. Chang and Gossard (1997) presented the transformation vectors to describe variation and displacement of features. They modeled the parts and tooling as groups of features. The method represented the interaction between parts and tooling by contact chains. A contact modeling algorithm implemented into the Method of Influence Coefficient to prevent penetrations between parts has been presented by Dahlström and Lindkvist (2007).

Non-contact 3D digitizing systems exposed a new horizon in geometric inspection of both rigid and nonrigid parts, because they deliver much more data than mechanical probes, in a shorter time. Weckenmann and Gabbia (2005) proposed a measuring method using virtual distortion compensation. Fringe projection systems are suitable for the fast and contact free measurement of parts without clamping. They used the measurement result to extract features of the object like holes or edges. Some of these were relevant for the assembly process; others were subject to further inspection. From the information about the transformation of the assembly features from their actual to their nominal position, virtual distortion compensation was used to calculate feature parameters of the distortion compensated shape.

Their method was not completely automated because the suggested method needed some human challenges to identify the correlation between some special points like holes and assembly joint positions. These led the controller to find the *boundary conditions* of the FEM problem. Besides, transforming the point cloud to a computer aided analyzable model is a very time-consuming process. It seems that this method is not suitable for really flexible parts because they have not considered the effect of gravity and the 3D situation which the part has scanned.

The concept of the *Small Displacement Torsor* (SDT) has been developed by Bourdet and Clément (1976) to solve the general problem of the fit of a geometrical surface model to a set of points using rigid body movements. Lartigue, Thiebaut et al. (2006) took advantage of the possibilities offered by voxel representation and SDT methods for dimensional metrology of flexible parts. This time, they considered the effect of gravity and spatial situation of a scanned part. This method is fundamentally based on finding the correlation between the cloud of all measured points and CAD meshed data. In fact, the SDT is more suitable for a small deformation. More accurate results can even be achieved if one considers the effect of material flexibility.

Abenhaim, Tahan et al. (2009) developed *iterative displacement inspection* (IDI) which smoothly deformed the CAD mesh data until matched to the range data. Their method was based on optimal step nonrigid ICP algorithms (Amberg, Romdhani et al. (2007)). The proposed IDI method was full of limitations. Their method was not tested in non-continuous areas such as holes, and the point cloud needed to be dense enough because the method's similarity measure was only based on the nearest distance calculation. The major flaw of this method was hidden in the fact that it strongly depended on finding some trials and prior flexibility parameters which could vary depending on thickness. Furthermore, the method supposes that the boundary of measured parts is without defect so the method is not suitable in the case of shrinkage. The mentioned drawbacks cause the IDI to be ineffective in real engineering applications.

Including *part compliance with intrinsic geometry of surface* in metrology of free-form surfaces, is an area of research pioneered in this thesis.

1.2 Rigid and nonrigid surface registration

Parallel to mechanical engineers but in different fields like *Computer science, Biomedical engineering* and *Pattern recognition*, tons of research has been done on Rigid and Nonrigid Registration and deformable surface comparison domains. Besl and McKay (1992) developed an iterative method for the rigid registration of 3D shapes. The idea behind the iterative closest point (ICP) algorithms is simple: given two surfaces, X and Y , find the rigid transformation (R, t) , so that the transformed surface $Y' = RY + t$ is as 'close' as possible to X . 'Closeness' is expressed in terms of some surface-to-surface distance $d(RY + t, X)$. More precisely, ICP can be formulated as a minimization problem:

$$d_{ICP}(X, Y) = \min_{R,t} d(RY + t, X) \quad (1.1)$$

This algorithm differs in the choice of the surface-to-surface distance $d(Y', X)$ and the numerical method for solving the minimization problem. The ICP algorithm is one of the common techniques for refinement of partial 3D surfaces (or models) and many variant techniques have been investigated. However, searching the closest point in the ICP algorithm is a computationally expensive task. In order to accelerate the speed of closest point searching, some search techniques are commonly employed. Many variants of ICP have been proposed, affecting all phases of the algorithm - from the selection and matching of points, to the minimization strategy. The correspondence between points is usually performed by a nearest-neighbour search using a k-d tree structure for optimization (Bentley (1975)). The k-d tree is a spatial data structure originally proposed to allow efficient search on orthogonal range queries and nearest neighbour queries (Bentley (1975)). Greenspan and Godin (2001) proposed a significant improvement in the nearest neighbour queries by using correspondences of previous iterations of the ICP and searching only in their small neighbourhood to update the correspondences. Another important strategy to speed up the

registration process uses sampling techniques to reduce the number of points in the views (Rusinkiewicz and Levoy (2001)).

Myronenko, Song et al. (2007) introduced a probabilistic method for rigid, affine, and nonrigid point set registration, called the *Coherent Point Drift algorithm*. They considered the alignment of two point sets as the probability density estimation, where one point set represents the Gaussian Mixture Model centroid, and the other represents the data point. They iteratively fitted the GMM centroids by maximizing the likelihood and found the posterior probabilities of centroids, which provide the correspondence probability. The method based on forcing the GMM centroids to move coherently as a group, preserved the topological structure of the point sets.

Schwartz, Shaw et al. (1989) were the first that used *Multidimensional Scaling (MDS)* methods to flatten the curved convoluted surfaces of the brain in order to study functional architectures and the neural maps embedded in them. For some, their work was a breakthrough in which surface geometry was translated into a plane. But the plane restriction introduced deformations that actually prevented the proper matching of convoluted surfaces. This problem can be solved if higher dimensions of the embedding space are considered.

The *Fast marching method* was introduced by Sethian (1996) as a computationally efficient solution to *Eikonal equations* on flat domains. A related method was presented by Tsitsiklis (1995). The fast marching method was extended to triangulated surfaces by Kimmel and Sethian (1998). The extended method solved Eikonal equations on flat rectangular or curved triangulated domains.

Elbaz and Kimmel (2003) presented a blend of topology and statistical methods, to introduce the concept of *Invariant signature* for surfaces. Their method was based on fast marching on triangulated domain algorithm followed by MDS technique. They have practically transformed the problem of matching isometric-nonrigid surfaces into the problem of matching of rigid surfaces. Using MDS, they embedded surfaces X and Y into some common

embedding space Z called *Canonical form* and then measured the similarities using the *Hausdorff distance*. Their method is strongly based on the Kimmel and Sethian (1998) method in computing the geodesic distance on triangular meshes.

Mémoli and Sapiro (2005) proposed a computational framework for comparing sub-manifolds given as point clouds. They considered *permutation distance* (d_p) the approximation of the *Gromov-Hausdorff* (d_{GH}) distance which has been embedded in a probabilistic framework. d_p can be considered as a particular discrete case of Gromov-Hausdorff distance. Their idea was based on selecting sub-samplings of the given point clouds, the distance between which could be related to the Gromov-Hausdorff distance.

In fact, Euclidean embedding is rarely without distortion. Cox (2000) showed how points of a configuration from a non-metric MDS can be forced to lie on the surface of a sphere. Replacing the Euclidean geometry of the embedding space with a spherical one usually gives smaller metric distortion but this distortion is still not zero. Bronstein, Bronstein et al. (2006) proposed a method. Instead of embedding X and Y into some common embedding space that introduced inevitable distortions, they embedded X directly into Y . In spite of the Elbaz and Kimmel (2003) method, they did not use canonical forms anymore and the distance between two surfaces was obtained from the solution of the embedding problem itself.

CHAPTER 2

THEORETICAL FOUNDATIONS

In this chapter, we introduce theoretical foundations that will allow us to formulate properties of nonrigid shapes.

2.1 Metric spaces

Definition 1: Let X be an arbitrary set. A function $d : X \times X \rightarrow \mathbb{R} \cup \{\infty\}$ is a metric on X if the following conditions are satisfied for all $x, y, z \in X$.

(1) *Positiveness:* $d(x, y) > 0$ if $x \neq y$ and $d(x, x) = 0$.

(2) *Symmetry:* $d(x, y) = d(y, x)$.

(3) *Triangle inequality:* $d(x, z) \leq d(x, y) + d(y, z)$.

A *metric space* is a set with a metric on it. In a formal language, a metric space is a pair (X, d) where d is a metric on X . Elements of X are called *points* of the metric space; $d(x, y)$ is referred to as the *distance* between points x and y .

Unless different metrics on the same set X are considered, we will omit an explicit reference to the metric and write “a metric space X ” instead of “a metric space (X, d) .”

Definition 2: Let X and Y be metric spaces with metrics d_X and d_Y . A map $f : X \rightarrow Y$ is called *distance preserving* if for any $a, b \in X$ one has $d_Y(f(a), f(b)) = d_X(a, b)$. Such a bijective distance preserving map is called an *isometry*, and two metric spaces related by such a map are referred to as *isometric*.

Definition 3: Let X and Y be metric spaces and $f : X \rightarrow Y$ an arbitrary map. The *distortion* of f is defined by:

$$\text{dis } f = \sup_{a, b \in X} |d_Y(f(a), f(b)) - d_X(a, b)| \quad (2.1)$$

The distance $d_X(a, b)$ between a pair of points in X is mapped to the distance $d_Y(f(a), f(b))$ between the images of a and b under f .

Definition 4: Let X be a length space. A curve $\gamma: I \rightarrow X$ is called a *geodesic* if for every $t \in I$ there exists an interval J containing a neighbourhood of t in I such that $\gamma|_J$ is a shortest path. In other words, a geodesic is a curve which is locally a distance minimizer (i.e. a shortest path).

Definition 5: Let A and B be subsets of a metric space (Z, d_Z) . The *Hausdorff distance* between A and B , denoted by $d_H(A, B)$, is defined by:

$$d_H(A, B) = \max \left\{ \sup_{a \in A} d_Z(a, B), \sup_{b \in B} d_Z(b, A) \right\} \quad (2.2)$$

Definition 6: *Gromov-Hausdorff distance* between two metric spaces (X, d_X) and (Y, d_Y) is defined as:

$$d_{GH}(X, Y) = \inf \{ d_H(X, Y) \} \quad (2.3)$$

where the infimum is taken over all (semi-)metrics on $X \cup Y$ extending the ones of X and Y . d_{GH} satisfies the triangle inequality, i.e. ,

$$d_{GH}(X_1, X_3) \leq d_{GH}(X_1, X_2) + d_{GH}(X_2, X_3) \quad (2.4)$$

for any metric spaces X_1, X_2, X_3 . Moreover $d_{GH}(X, Y) = 0$ if and only if X and Y are isometric.

Definition 7: Let \mathfrak{R} be a correspondence between metric spaces X and Y . The distortion of \mathfrak{R} is defined by:

$$\text{dis } \mathfrak{R} = \sup \{ |d_X(x, x') - d_Y(y, y')| : (x, y), (x', y') \in \mathfrak{R} \} \quad (2.5)$$

For any two metric spaces X and Y ,

$$d_{GH}(X, Y) = \frac{1}{2} \inf_{\mathfrak{R}} (\text{dis } \mathfrak{R}) \quad (2.6)$$

where the infimum is taken over all correspondences \mathfrak{R} between X and Y .

2.2 Point cloud techniques

A point cloud is a set of vertices in a three-dimensional coordinate system created by 3D scanners. Point clouds themselves are generally not directly usable in most 3D applications, and therefore are usually converted triangle mesh models, NURBS models, or CAD models. *Numerical geometry* is the branch of computer science that studies algorithms and data structures for problems stated in terms of geometrical objects.

2.2.1 Smoothing of noisy data

There are two types of digital measurement techniques: contact measurement using a coordinate measuring machine (CMM), and noncontact measurement, such as laser and optical scanning. Non-contact measuring methods are of a significantly higher speed and have been widely used. Unfortunately, some of the point cloud data obtained by non-contact approach do not reflect the right location on the real surface due to physical noise added by the technical scanning device. It is necessary to smooth point cloud data in the inspection of free-form surfaces, because noisy points will have a negative influence on the post-processing of this data. The big problem in smoothing point cloud data is how to solve the dilemma between removing noisy points while preserving the underlying sampled surface, in particular its fine features. Denoising the ranged data can be applied either before or after mesh generation. The advantage of denoising the mesh rather than a point cloud is that the connectivity information implicitly defines the surface topology and serves as a tool for fast access to neighbouring samples. It is evident that the noise in range data will affect the proposed methods, but study of these effects as well as the diverse smoothing methods may be the subject of future research. In this thesis we will deal with noiseless data.

2.2.2 Point cloud sampling

Imagine that we were to establish a number of TV/ radio stations all over Quebec. On one hand, the stations would have to be placed sufficiently densely to provide good coverage of the territory. On the other hand, the installation of each station costs millions of dollars.

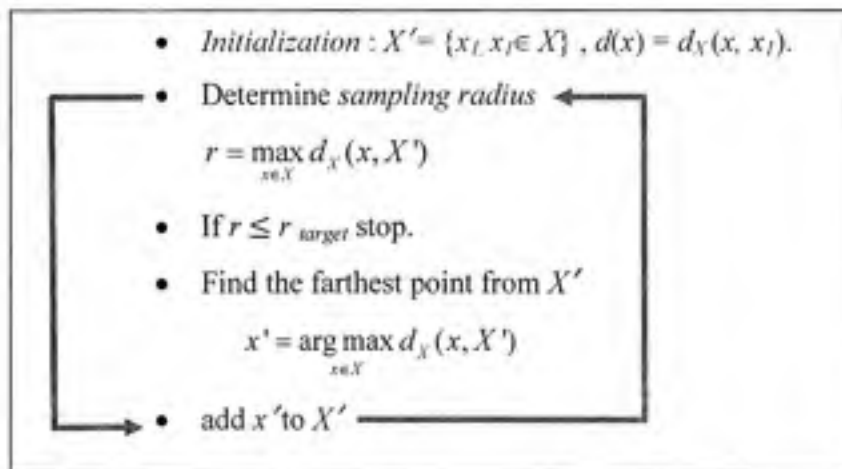
Therefore, we are interested in having the network as sparse as possible. *Sampling* is one of the most basic problems in discrete surface representation. On one hand, in order to better represent the underlying surface, we prefer the sampling to be as densely as possible, and on the other hand, we need to keep in mind that the discrete representation is used by computer algorithms, and every additional point increases storage and computational complexity costs. Let's continue with our TV/ radio station problem. We start by placing the first station at a point x_1 . The second station should be placed as far as possible from the first one:

$$x_2 = \arg \max_{x \in X} d_X(x, x_1) \quad (2.7)$$

The third station will be placed at the maximum distance from x_1 and x_2 , i.e.,

$$x_3 = \arg \max_{x \in X} d_X(x, \{x_1, x_2\}) \quad (2.8)$$

and so on. The described algorithm is well known as the *farthest point sampling* (FPS) algorithm and summarized below:



Algorithm 1 Farthest point sampling algorithm.

In our example we can approximate $d_X(x_1, x_2)$ as Euclidean distance; this conveys the extrinsic geometry of the surface. However, because a surface is also characterized by an intrinsic geometry such a discretization, it is incomplete until the length and the metric structures are also discretized. In other words, we should approximate the intrinsic geometry of our surface. This will be discussed in upcoming sections.

2.2.3 Fast marching method

In this section we are going to compute the geodesic distance in a discretized surface. This is extremely important to approximate the intrinsic geometry of our surface. If our sampled domain is dense enough, one idea is to approximate the geodesic distance between points with the famous *Dijkstra's shortest path algorithm* (Dijkstra (1959)). In fact, the shortest path computed by Dijkstra's algorithm does not always lead to the real shortest path. This inconsistency is due to the fact that we are allowed to move in the graph only parallel to the axes.

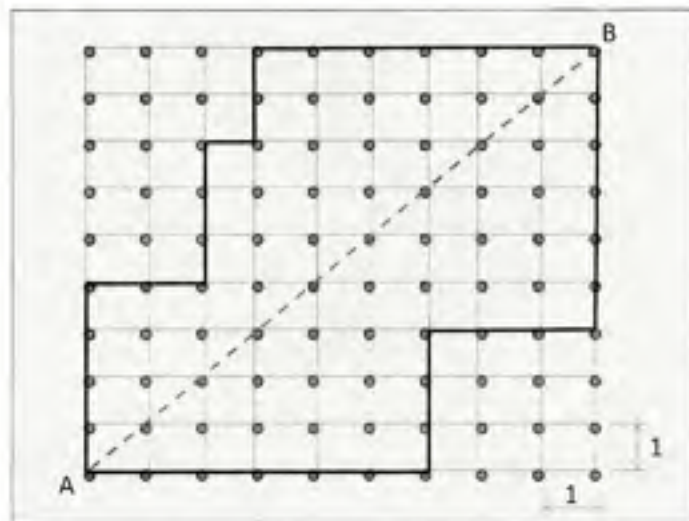


Figure 2.1 Shortest paths computed by Dijkstra's algorithm.

As shown in Figure 2.1, the shortest paths computed by Dijkstra's algorithm (solid black lines), between A and B never converge to the true shortest path (dashed line). This implies using another algorithm, without being restricted to the edges. Such algorithms, called the *fast marching method*, were introduced by Sethian (1996). Sethian's fast marching method is a numerical algorithm for solving the *Eikonal equation* on a rectangular orthogonal mesh. Later on, Kimmel and Sethian (1998) extended the fast marching method to triangulated domains with the same computational complexity. Here, we focus on the latter algorithm.

Consider a boundary, either a curve in two dimensions or a surface in three dimensions, separating one region from another. Imagine that this curve/surface moves in a direction normal to itself (where the normal direction is oriented with respect to an inside and an outside) with a known *speed function* F . Given F and the position of an interface, the objective is to track the evolution of the interface. Assume for the moment that $F > 0$, hence the front always moves *outward*. One way to characterize the position of this expanding front is to compute the arrival time $T(x, y)$ of the front as it crosses each point (x, y) , as shown in Figure 2.2.

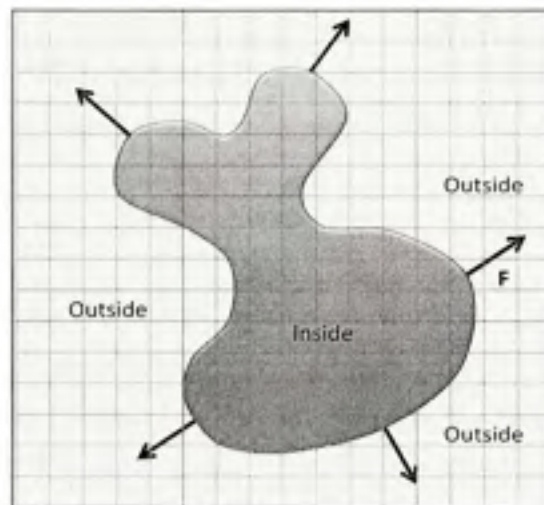


Figure 2.2 Calculation of crossing time at (x, y) for expanding front $F > 0$.

The equation for this arrival function $T(x, y)$ is easily derived. In one dimension, using the fact that *distance = rate * time* (see Fig 2.3), we have the following:

$$1 = F \frac{dT}{dx} \quad (2.9)$$

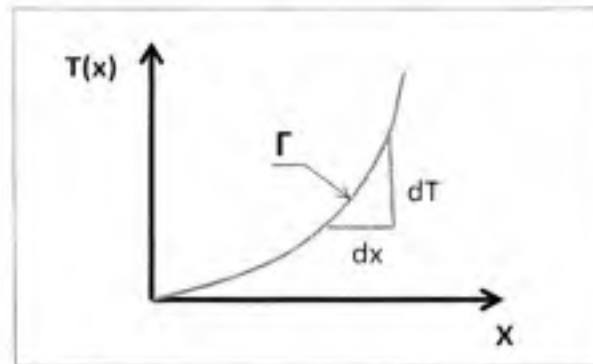


Figure 2.3 Setup for boundary value formulation.

In multiple dimensions, ∇T is orthogonal to the level sets of T , and, similar to the one-dimensional case, its magnitude is inversely proportional to the speed. Hence:

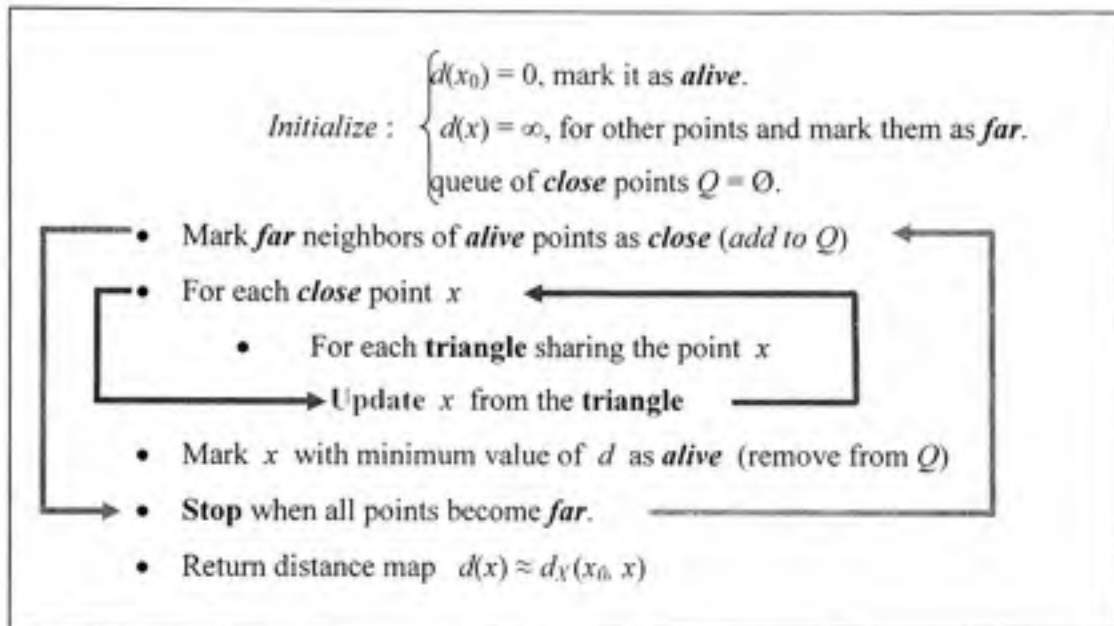
$$|\nabla T|F = 1, \quad T = 0 \text{ on } \Gamma \quad (2.10)$$

where Γ is the initial location of the interface. Thus, the front motion is characterized as the solution to a boundary value problem. If the speed F depends only on position, then the equation reduces to what is known as the *Eikonal equation*. So our goal is to construct algorithms to solve the Eikonal equation. The following approximation of the gradient magnitude results in a monotone scheme that selects the viscosity solution (Rouy and Tourin (1992)):

$$\left[\begin{array}{l} \max(D_{\partial k}^{-} T, -D_{\partial k}^{+} T, 0)^2 \\ + \max(D_{\partial l}^{-} T, -D_{\partial l}^{+} T, 0)^2 \\ + \max(D_{\partial m}^{-} T, -D_{\partial m}^{+} T, 0)^2 \end{array} \right]^{1/2} = \frac{1}{F_{\partial k}} \quad (2.11)$$

The standard methods for the boundary value view require iteration. Sethian described *Fast Marching Methods*, which allow one to solve the boundary value problem without iteration. Technically, it is a dynamic programming sequential estimation method, very similar to Dijkstra's algorithm. Fast marching keeps for each point x on the mesh the time of arrival $d(x)$ of the wave front originating in x_0 (Figure 2.4). We can freely switch between the path length and arrival time. The initial approximation of $d(x)$ is, like in *Dijkstra's algorithm*, zero at x_0 and infinity elsewhere. The algorithm classifies the points of the mesh into three

categories: *Alive*, *Close* and *Far*. The Fast Marching Method algorithm is as follows: first, tag points in the initial conditions as *Alive*. Then tag as *Close* all points one grid point away. Finally, all other grid points are tagged as *Far*.



Algorithm 2 Fast marching algorithm.

The main difference with Dijkstra's algorithm is hidden under the *update* step. In Dijkstra's algorithm the path was restricted to the graph edges, and a graph vertex was updated each time from an adjacent vertex. In fast marching, because the path can pass through the triangular faces of the mesh, a vertex has to be updated from a triangle, requiring two supporting vertices.

Suppose that the front reaches to x_1 at time d_1 and to x_2 at time d_2 (Fig 2.4). Now we want to estimate the time when the front arrives to x_3 . The discretization of the Eikonal equation, considering a linear approximation leads to the following quadratic equation:

$$d_3^2 \cdot 1^T Q 1 - 2d_3 \cdot 1^T Q d + d^T Q d - 1 = 0 \quad (2.12)$$

Where $d = (d_1, d_2)^T$, $V = (x_1, x_2)$, $1 = (1, 1)^T$ and $Q = (V^T V)^{-1}$.

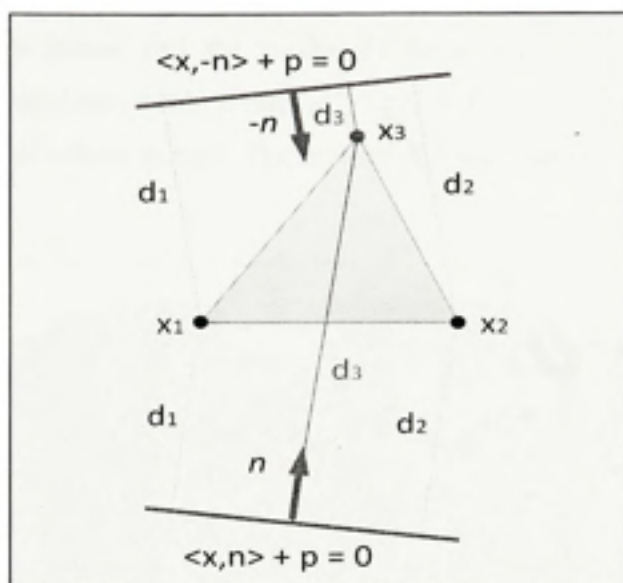


Figure 2.4 Quadratic equation is satisfied by both n and $-n$.

Without going into detail, this entire update step can be summarized in Algorithm 3.

- Solve the quadratic equation and select the largest solution:

$$d_3^2 \cdot 1^T Q 1 - 2d_3 \cdot 1^T Q d + d^T Q d - 1 = 0$$

- Compute the front propagation direction:

$$n = V^{-T} (d - d_3 \cdot 1)$$

- if $QV^T n < 0$

$$d(x_3) = \min\{d(x_3), d_3\}$$

$$d_3 = \min\{d_1 + \|x_1 - x_3\|_2, d_2 + \|x_2 - x_3\|_2\}$$

Algorithm 3 Fast marching update.

We applied both the fast marching method and Dijkstra's algorithm to our first case study, between two arbitrary points, and the results are presented in Fig. 2.5. The green line represents Dijkstra's algorithm which results in 2.1098 m and never converges to the red line calculated by the fast marching method. The shortest path calculated by FMM is 2.0427 m .

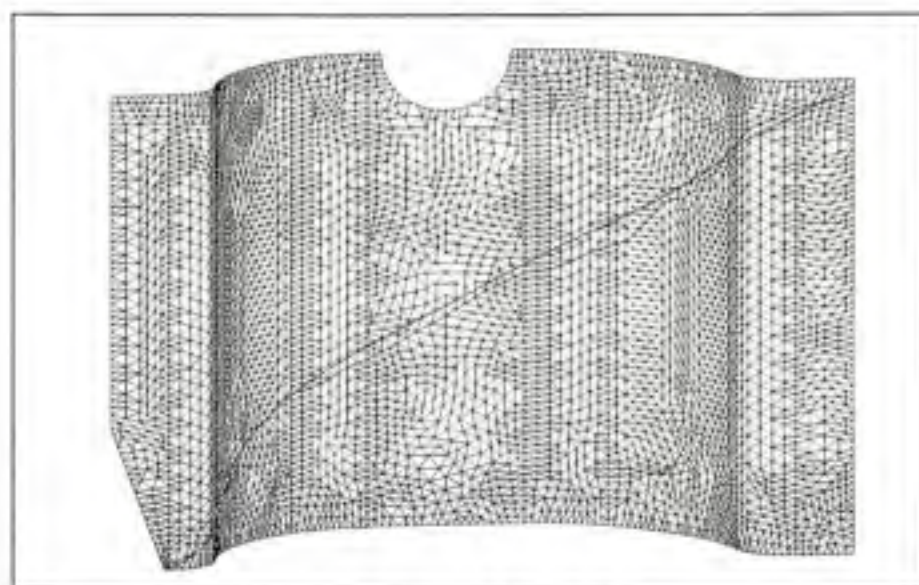


Figure 2.5 Comparison between FMM and Dijkstra's algorithm.

2.3 Isometric embedding

As we said in section 2.1, intrinsic geometries rest unchangeable compared to isometric deformations. In order to compare nonrigid shapes we should look at their intrinsic geometries. Consider the shapes in Fig. 2.6 as metric spaces. Shapes (b) and (c) belong to the same metric space \mathbb{R}^3 . Therefore, we can measure their similarity using the *Hausdorff distance*, which leads us to a well-known ICP algorithm. Now consider the shapes (a) and (b) with the geodesic metrics d_X and d_Y respectively. In this case, we have two different metric spaces (X, d_X) and (Y, d_Y) which cannot be compared using Hausdorff distance. In other words, Hausdorff distance is not isometry-invariant.

Now, consider the shape (X, d_X) , and a map like: $f : (X, d_X) \rightarrow (\mathbb{R}^m, d_{\mathbb{R}^m})$ such that:

$$d_Y(x, x') = d_{\mathbb{R}^m}(f(x), f(x')) \quad (2.13)$$

for all $x, x' \in X$. A map like f is an *isometric embedding* and space like \mathbb{R}^m called as *embedding space*. The term *canonical form*, computed as Hausdorff distance between the minimum distortion embeddings of two shapes X and Y into some common metric space (Z, d_Z) , are used as well. In fact, canonical form is the extrinsic representation of the intrinsic geometry of shape X , and using this, we can transform our nonrigid shape similarity into the rigid similarity problem. We used \mathbb{R}^3 ($m = 3$) as embedding space, but this method can be generalized to any embedding space. However, the problem is whether a shape like X is isometrically embedded into \mathbb{R}^m .

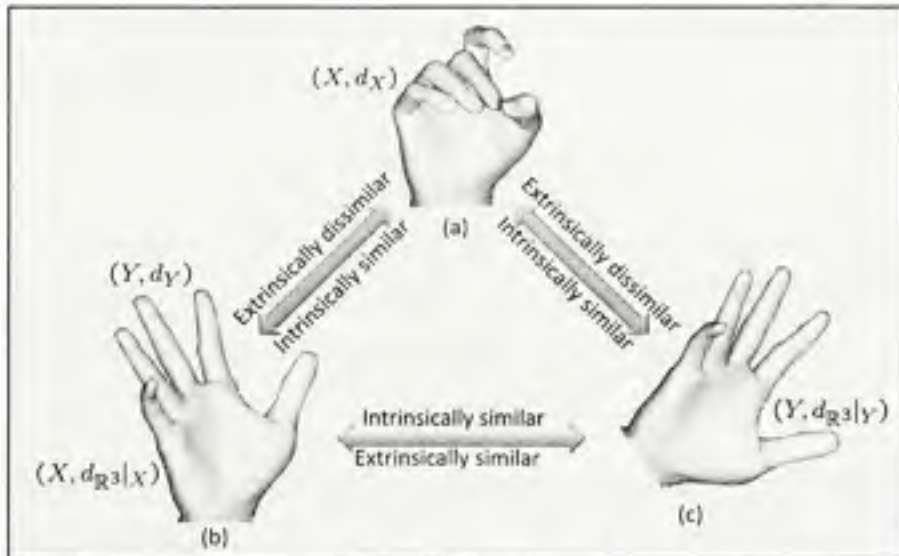


Figure 2.6 Difference between intrinsic and extrinsic similarity.

In real world applications, the answer is usually negative. Recalling our knowledge of differential geometry, we know that *Gaussian curvature* is an intrinsic invariant of a surface. As an example, a sphere of radius r has constant Gaussian curvature which is equal to $1/r^2$. At the same time, a plane has zero Gaussian curvature. As a corollary of Gauss' *Theorema Egregium* (Latin: "Remarkable Theorem"), a piece of paper cannot be bent onto a sphere

without crumpling. Conversely, the surface of a sphere cannot be unfolded onto a flat plane without distorting the distances.

Although a truly isometric embedding of shape X is not always possible, we can try to construct an approximate representation of X minimizing *distortion* as we defined in equation (2.1):

$$\text{dis } f = \sup_{x, x' \in X} |d_{\mathbb{R}^m}(f(x), f(x')) - d_X(x, x')| \quad (2.14)$$

In our point cloud setting, where the shape X is sampled at N points $\{x_1, x_2, \dots, x_N\}$, the distortion criteria will be:

$$\sigma = \max_{i, j \in \{1, \dots, N\}} |d_{\mathbb{R}^m}(f(x_i), f(x_j)) - d_X(x_i, x_j)| \quad (2.15)$$

The function σ which measures the distortion of distances is called *stress*. As a routine σ_2 is used as the distortion criterion. Considering $Z_i = f(x_i)$ an $N \times m$ matrix of canonical form coordinates and $d_g(Z) = d_{\mathbb{R}^m}(z_i, z_j)$:

$$\sigma_2(Z; D_X) = \sum_{i > j} |d_g(Z) - d_X(x_i, x_j)|^2 \quad (2.16)$$

Where $D_X = d_X(x_i, x_j)$ is a $N \times N$ matrix of geodesic distances and $d_g(Z)$ is the Euclidean distance between the points on the canonical form. Using this formulation the coordinates of discrete canonical form is the solution of nonlinear least-squares problem:

$$Z^* = \arg \min_{Z \in \mathbb{R}^{N \times m}} \sigma_2(Z) \quad (2.17)$$

and the minimization algorithms known as *Multidimensional scaling* that are closely related to *dimensionality reduction*.

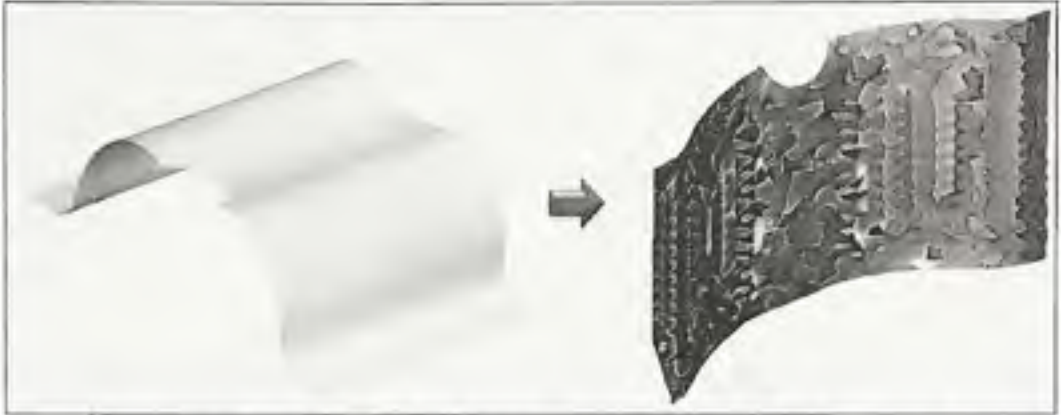


Figure 2.7 Applying the SMACOF algorithm to the first case study.

Elbaz and Kimmel (2003) used a SMACOF algorithm to minimize stress function. In Annex II, we have represented MATLAB codes applied to our first case study. We tried to construct an approximate representation of our first case study, minimizing the distortion. Sampling the part with 1267 vertices and with 20 iterations, we reduced the stress from $1.87e+4$ to 168. Fig 2.7 represents the results of this applied method. In the next section we are going to look at some deep aspects of the GMDS algorithm.

2.4 Generalized multidimensional scaling

The idea is to find the minimum distortion embedding of X into Y which allows us to quantify the dissimilarity of the intrinsic geometries of two surfaces. The lowest achievable distance can be demonstrated as embedding distance:

$$d_E(Y, X) = \inf_{f: X \rightarrow Y} \text{dis } f \quad (2.18)$$

Remind the prototype MDS problem with σ_2 stress as:

$$\min_{z_1, \dots, z_n \in \mathbb{R}^k} \sum_{i < j} |d_Y(Z_i, Z_j) - d_X(x_i, x_j)|^2 \quad (2.19)$$

Here the minimizer is the canonical form of the shape X and the minimum is the embedding distortion (σ_2). In practice, the distortion is non-zero, but yet it can be reduced by finding a better embedding space. Cox (2000) showed how points of a configuration from non-metric MDS can be forced to lie on the surface of a sphere. Replacing the Euclidean geometry of the

embedding space with a spherical one usually gives smaller metric distortion, but still this distortion is not zero. Bronstein *et al.* (2006) proposed a method. Instead of embedding X and Y into some common embedding space \mathbb{Z} that introduced inevitable distortions, they embedded X directly into Y . In other words, they embed X into Y by solving the following problem:

$$\min_{y'_1, \dots, y'_M \in Y} \sum_{i,j} |d_Y(y'_i, y'_j) - d_X(x_i, x_j)|^2 \quad (2.20)$$

We denote the image of x_i in Y as y'_i . The minimum stress value measures how much the metric of X should be distorted in order to fit into Y . Now there is no more need to compare canonical forms and the dissimilarity is obtained directly from the embedding distortion.

At first glance GMDS seems like an extraordinary idea for isometric invariant surface matching problems. But in practice it presents a new set of challenges. Unlike the Euclidean or the spherical cases, we have no more closed-form expression for $d_Y(y'_i, y'_j)$ and metric needs to be approximated as y'_i are the optimization variables. Consider Y sampled at $Y_M = \{y_1, \dots, y_M\}$ and represented as a triangular mesh $T(Y_M)$. So any point $y'_i \in Y_M$ falls into one of the triangles $t_i \in T$ (t_i is the triangle index). Using the *convex combination* of triangle vertices $x_{t_{i,1}}, x_{t_{i,2}}, x_{t_{i,3}}$:

$$y'_i = u_i^1 x_{t_{i,1}} + u_i^2 x_{t_{i,2}} + u_i^3 x_{t_{i,3}} \quad (2.21)$$

where $u_i^1 + u_i^2 + u_i^3 = 1$ and $y'_i = (t_i, u_i)$ are *Barycentric coordinates*. Especially for complicated surfaces, finding an accurate continuous *global* parameterization is probably impossible, so a *local* parameterization is presented, although it is needed to handle discrete indices t_i in minimization algorithm. Using FMM, distance terms $d_X(x_i, x_j)$ can be precomputed; the question is how to compute distance terms $d_Y(y'_i, y'_j)$. Bronstein, Bronstein *et al.* (2007) proposed the *three point geodesic distance interpolation*. They precomputed $(D_Y)_{ij} = d_Y(y_i, y_j)$ and in a four-step approach showed that:

$$\hat{d}_Y(y, y') = u'^T D_Y(t, t') u \quad (2.22)$$

Using the previous equation and substituting in the generalized σ_2 stress function,

$$\sigma_2(u_i) = \sum \left(d_x(x_i, x_j) - u_i^T D_r(t_i, t_j) u_j \right)^2 \quad (2.23)$$

Stress as a function of u_i is quadratic: $\sigma(u_i) = u_i^T A_i u_i + 2b_i^T u_i + c_i$, which,

$$A_i = \sum_{j \neq i} D_r(t_i, t_j) u_j u_j^T D_r(t_i, t_j)^T \quad (2.24)$$

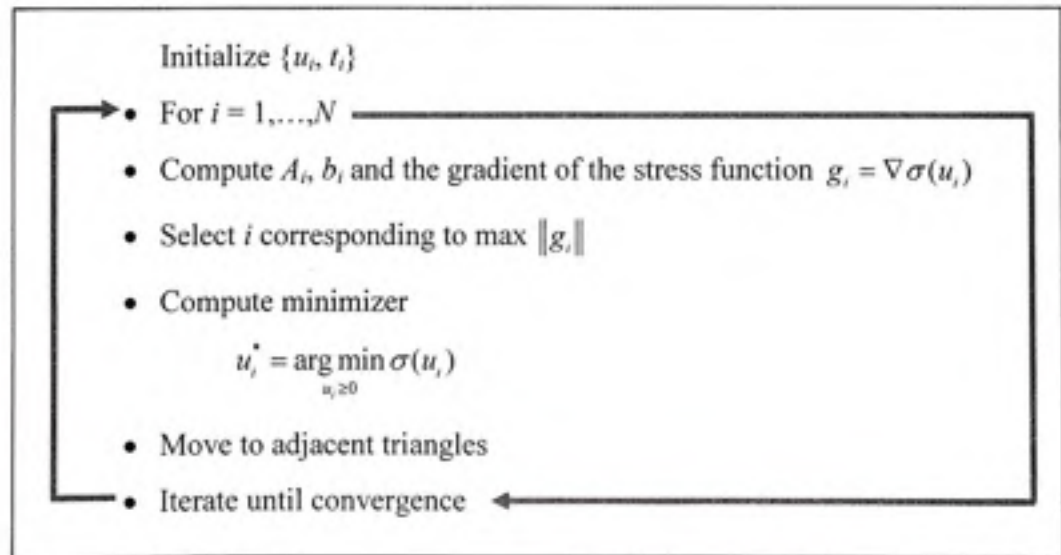
$$b_i = - \sum_{j \neq i} d_x(x_i, x_j) D_r(t_i, t_j) u_j \quad (2.25)$$

$$c_i = \sum_{j \neq i} d_x^2(x_i, x_j) \quad (2.26)$$

The closed-form solution for minimizer of $\sigma(u_i)$ is:

$$u_i^* = \arg \min_{u_i} \sigma(u_i) = \arg \min_{u_i} u_i^T A_i u_i + 2b_i^T u_i + c_i \quad (2.27)$$

In order for such a solution not to be outside the triangle, the minimizer should be so that, $u_i \geq 0$ and $u_i^1 + u_i^2 + u_i^3 = 1$. Without going into detail, the least square GMDS can be summarized in Algorithm 4.



Algorithm 4 GMD

In Figure 2.8 we tried to construct a simplified representation of all the algorithms presented until now. The total number of point clouds in two shapes X and Y are represented by n and m , respectively. D_X and D_Y represent symmetric matrixes of pairwise geodesic distances with $a_{ii} = 0$, calculated by fast marching method.

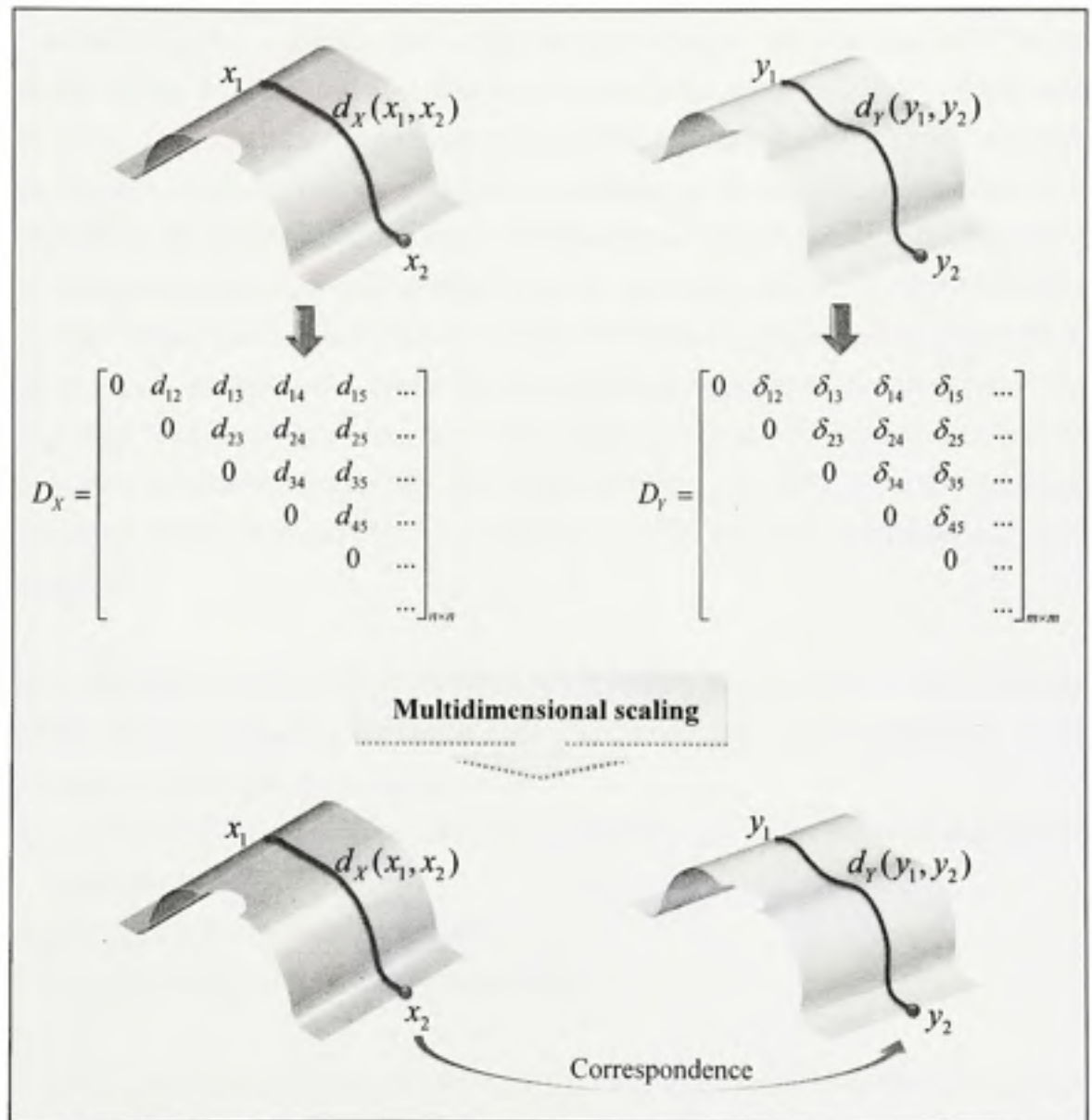


Figure 2.8 Simplified representation of similarity measure.

CHAPTER 3

NONRIGID GEOMETRIC INSPECTION

3.1 Geometry of flexible parts

Free-state variation is a term used to describe part distortion after the removal of forces applied during manufacture. This distortion is principally due to the part's weight and flexibility and the release of internal stresses resulting from fabrication. A part of this kind, for example, a part with a very thin wall in proportion to its diameter, is referred to as a nonrigid part (ASME Y14.5). As a state of weightlessness is rarely possible, the shape of an assembly component is generally defined in the *use state* when joined with other parts. This use state defines the boundary conditions, which will define the constrained geometry. When the boundary conditions are applied to the theoretical *free shape*, the geometry of the assembled component is identical to a CAD model and this theoretical free shape can be analyzed with finite element method. The actual free shape is not as the same as a theoretical free shape, because it is not possible to elaborate its exact geometry; it includes *geometric deviation*.

Two methods are defined for the tolerancing of flexible parts according to ISO 10579 and ASME Y14.5: tolerancing at the free-state and tolerancing under constraints. Three indications must be taking into consideration:

- 1) Condition of boundary constraints, such as assembly constraints and/or external forces, including gravity.
- 2) Acceptable deviations at the free-state.
- 3) Acceptable deviations at the constrained state.

The free-state does not correspond to the state of weightlessness which we named free shape. Besides, in ISO 10579, the position of the part in regard to the direction of the gravity is clearly defined and it is notable that the tolerance values are greater in the free-state than in the constrained state which generally corresponds to the use state. (Fig 3.1)

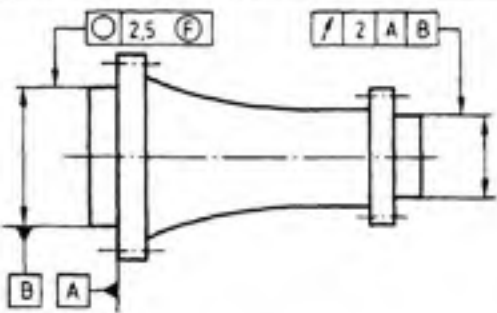
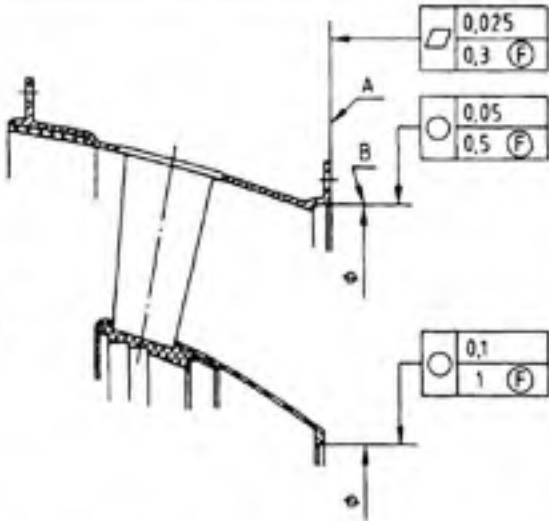
| Indication sur le dessin | Interprétation |
|--|---|
|  <p>ISO 10579-NR</p> <p>Condition de contrainte: la surface indiquée comme référence spécifiée A est montée (avec 64 boulons M6 serrés avec un couple de 9 N·m à 15N·m) et l'élément indiqué comme référence spécifiée B est contraint à la limite maximale du matériau correspondante.</p> | <p>La tolérance géométrique suivie du symbole \textcircled{M} doit être assurée à l'état libre. L'autre tolérance géométrique s'applique suivant les conditions indiquées dans la note.</p> |
|  <p>ISO 10579-NR</p> <p>Condition de contrainte: la surface repérée A est montée (avec 120 boulons M20 serrés avec un couple de 18 N·m à 20 N·m) et l'élément repéré B est contraint à la limite maximale du matériau correspondante.</p> | <p>Les tolérances géométriques suivies du symbole \textcircled{M} doivent être assurées à l'état libre. Les autres tolérances géométriques s'appliquent suivant les conditions indiquées dans la note.</p> |

Figure 3.1 Indication and interpretation of ISO 10579.

The condition that occurs when a cold-worked metal part has a tendency to partially return to its original shape is called *spring-back*. This is because of the elastic recovery of the material when the forming force is released. This severely affects the dimensional accuracy of the

part. Figure 3.2 schematically illustrate the effects of spring-back during dimensional metrology.

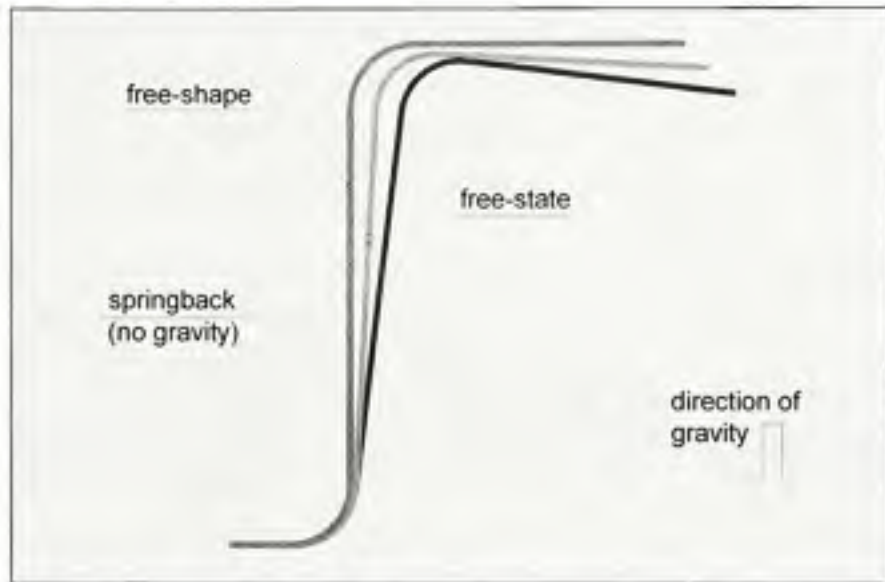


Figure 3.2 Effect of spring-back during geometrical inspection.

Levy (1984) indicated that Traditional trial-and-error methods are time-consuming and expensive, while empirical rule-based adjustments for spring-back are not usually applicable to complex geometries or materials without a large database of experience. Non-finite-element analytical methods have been applied to spring-back in die forming, often with limitations. Nowadays, finite element methods are used for analysing and predicting spring-back. Due to the fact that Spring-back is sensitive to a range of material and process parameters, such as strain hardening , evolution of elastic properties , elastic and plastic anisotropy and the presence of a Bauschinger effect (Li, Carden et al. (2002)) using these predicts in geometrical metrology may affect the accuracy of measurement. The quantity of this influence needs additional research. But what is clear is that doing finite element analysis for each production process is related to knowing the forming tool specification. For analysing complicated surfaces this is a very time-consuming process. However, the proposed inspection method should be capable of explaining the material behaviour during

registration between free-state (point cloud) and free-shape (nominal CAD data) states effectively.

As we discussed before, the *compliance* of a part is determined by the material properties and the geometry. Generally speaking, as shown in Fig. 3.3, three zones can be specified. Talking about the borders of these areas is a very vague concept, but in general, for the parts in “Zone C” the spring-back effect is negligible in comparison to the gravity effect.

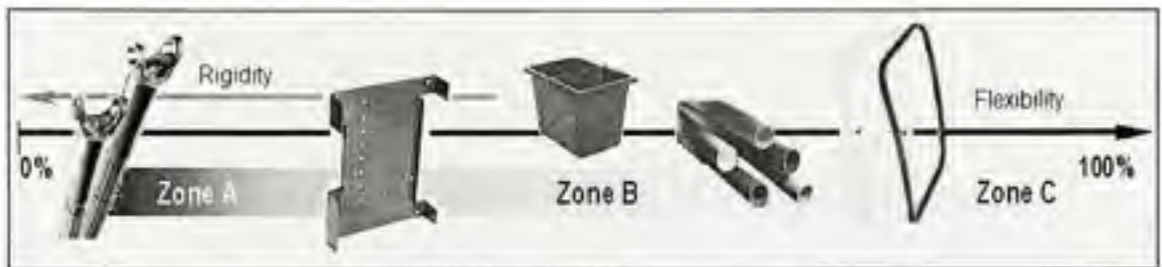


Figure 3.3 Classification of rigidity of parts.

Computer aided inspection methods used for geometric inspection of parts at zone A are based on *rigid surface registration* algorithms, such as the well-known ICP algorithm. In the next two sections we are going to develop a general methodology concerning materials belonging to zones C and B, respectively.

3.2 Identification of geometrical deviation

Various computer aided design and analysis softwares allow the inspector to easily obtain the point cloud from a CAD model. Assuming the availability of a scanned point cloud, our goal is to register two clouds of points. The first belongs to a CAD model and the second belongs to range data obtained in free-state. For flexible parts and before scanning, one should take into consideration the effect of spatial positioning (part set-up) in the final geometrical form of scanned data. Without knowing this important fact (gravity direction), serious errors in results can be predicted. Thus, before scanning, the part is set-up onto reference support points in which their position is clearly defined within the part frame. Note that, the set-up

must not be over constrained, unless otherwise specified according to designer demand (ISO 10579). In this case, the same constraints must be taken into consideration during finite element analysis.

Let x_1, x_2 be the theoretical points obtained within a CAD model, and x'_1, x'_2 the correspondence obtained from a finite element analysis and finally y'_1, y'_2 be the correspondence of two premier points in range data as shown in Figure 3.4.

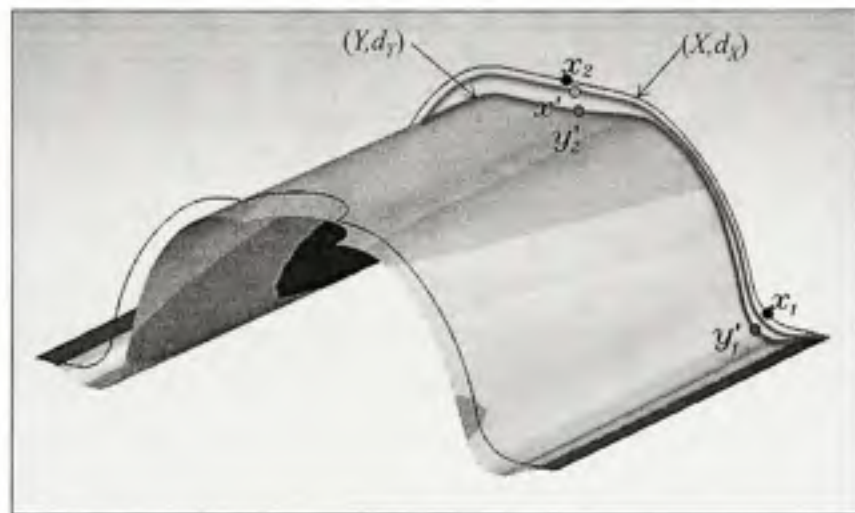


Figure 3.4 Measured point vs. FEM analysis and CAD data.

Assuming linearity, for the geometrical deviation, the following equation can be derived:

$$[R_{real}] = [R_{measured}] - [R_{theoretical}] \quad (3.1)$$

which $[R_{measured}] = x_i y'_i$ is the geometrical deviation between point clouds of CAD model and the measured surface. $[R_{theoretical}] = x_i x'_i$ is resulted from the finite element simulation of part in free-shape state in addition to gravity. As mentioned before, the same set-up constraints applied into scanning process must be taken into consideration as boundary conditions. At this stage real geometrical deviation $[R_{real}]$ can be calculated.

Correspondence between x_i and x'_i is evident; the challenge is how to find the y'_i which corresponds to x_i . Let X and Y be metric spaces with metrics d_X and d_Y ; the first correspond to a free-shape CAD model and the second to scanned range data. Due to the fact that x_i and y_i belong to two different metric spaces; similarity measure cannot be computed using Hausdorff distance algorithm. Remember that our deformation is a distance-preserving one, that is to say $d_X(x_i, x_j) = d_Y(y'_i, y'_j)$. Thus, our goal is to find a mapping like $f: X \rightarrow Y$, by solving the following problem:

$$\min_{y'_i \rightarrow y'_j \in Y} \sum_{i < j} |d_Y(y'_i, y'_j) - d_X(x_i, x_j)|^2 \quad (3.2)$$

where the y'_i is the image of x_i in Y . The minimum stress value measures how much the metric of X should be distorted in order to fit into Y . To this end, GMDS can be used to find the correspondence between simulated CAD and scanned clouds of points. $D_X = d_X(x_i, x_j)$ and $D_Y = d_Y(y_i, y_j)$ are the $n \times 3$ and $m \times 3$ matrix of geodesic distances computed by fast marching method in triangulated surfaces. Note that embedding process do not need primary surfaces registration (X and Y are different metric spaces). In this case, registration will be done on reference support points in which the position is clearly defined within the part frame, and this will occur before a geometric deviation calculation. Also note that a meshed CAD-model and scanned workpiece may have a different number of vertices. In this case, as discussed in chapter 2.4, a *three point geodesic distance interpolation* must be applied.

3.3 New definition for maximum geometric deviation

Normally the *maximum deviation* for geometric inspection is defined as the distance from a sensed point to the *substitute element*. Nowadays as there is no similarity measure tool between the CAD-model and range data the computer aided inspection software usually uses the maximum point-to-surface distance for maximum deviation calculation. GNIF, which will be presented in the next two chapters, will give us the capacity to deal with actual point-to-point geometric deviation. Fig 3.5 demonstrates the difference between the two kinds of geometric deviation calculations. The blue dimension line represents conventional geometric deviation and the red one represents actual geometric deviation.

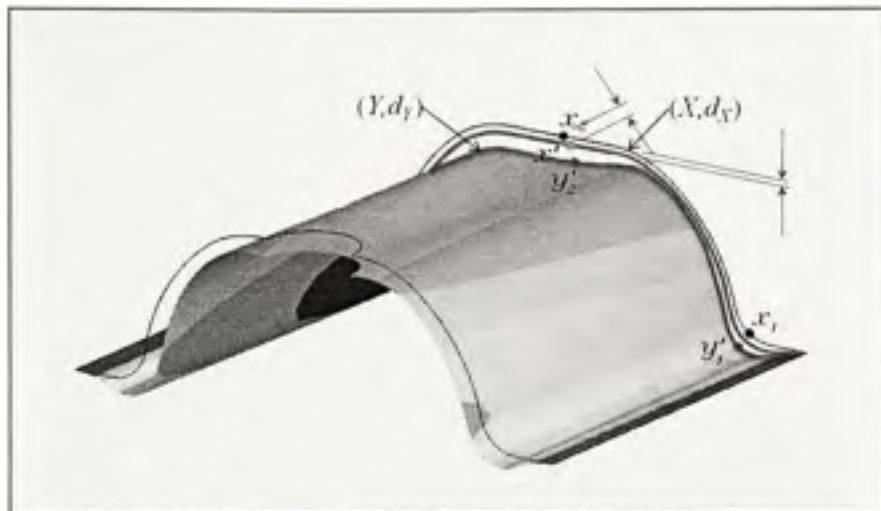


Figure 3.5 Actual and conventional geometric deviation.

3.4 Numerical inspection fixture

In today's industry, for geometric inspection of flexible parts, *inspection fixtures* in combination with coordinate measuring systems (CMM) are used. *Modular fixturing* is an essay for reducing the expensive costs of dedicated geometric inspection fixtures (Fig. 3.6). The part is set-up on the fixture, simulating the use state. To this end, offset and center locating elements together with CAD designed contour parts and quick clamps are used (Fig. 3.7). Their duty is to fix the distorted parts in a manner to eliminate the spring-back effects simulating the use state. Regardless of the many essays about the automation of geometric inspection process, 100% testing of all parts in mass production is impossible. In spite of sampling inspection (statistical control) for geometrical metrology of such product, this is still a time-consuming process. Our goal is to substitute the conventional fixtures with numerical ones.

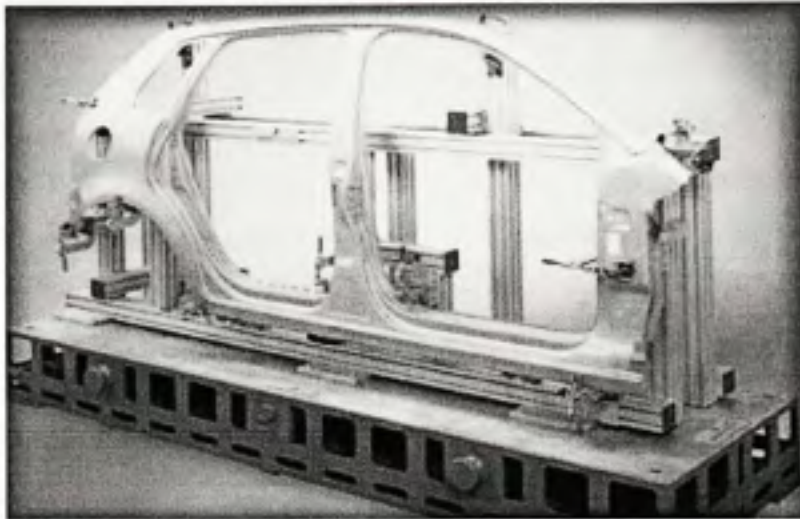


Figure 3.6 Dedicated inspection fixture for outer panel.
(BLUCO Corporation)³

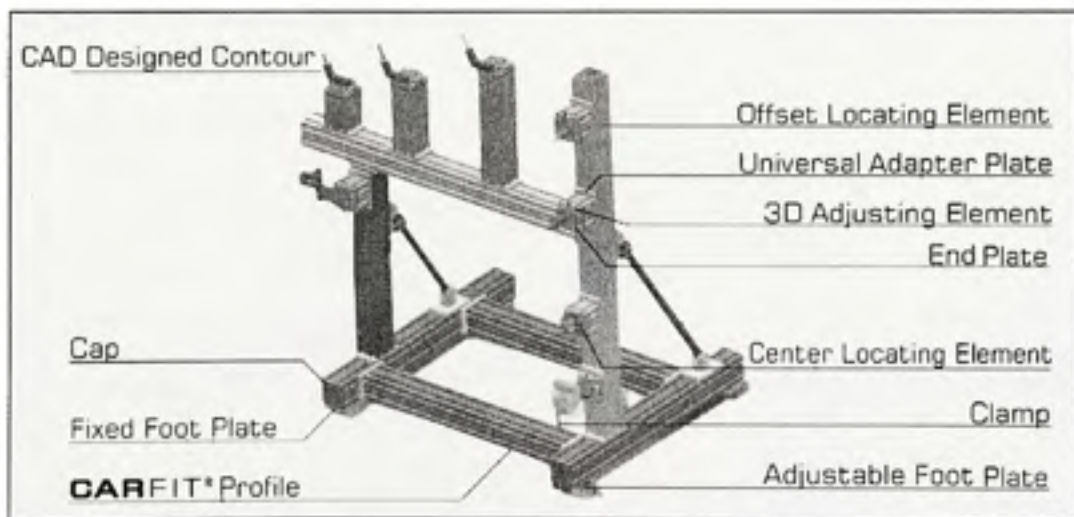


Figure 3.7 Details of inspection fixture.
(BLUCO Corporation)³

³ <http://www.bluco.com/>

To this end, the part is set-up onto reference support points for which the position is clearly defined within the part frame. These points, as priori information, will be utilized as the boundary condition, where it will simulate the gravity and support effect on the CAD-model. The workpiece is scanned in a distorted state without a fixation device. Two ways are possible to find the real geometrical deviation. The range data, including information about the assembly of the workpiece is processed. With this information about the use state, boundary conditions and the material properties, a FEM analysis is performed. The same gravity direction is applied to a free-shape CAD model. In other words, we use CAD free-shape model as a *Numerical Fixture* and processed range data will be fixed on it. The last step is a comparison between fixed processed range data and numerical fixtures. For complicated surfaces or surfaces with reinforced hidden ribs which are under scanned surfaces, the segmentation and modeling of range data is as time-consuming as conventional methods. Recent methods have been previously proposed by Weckenmann and Gabbia (2005); we just added a gravity effect..

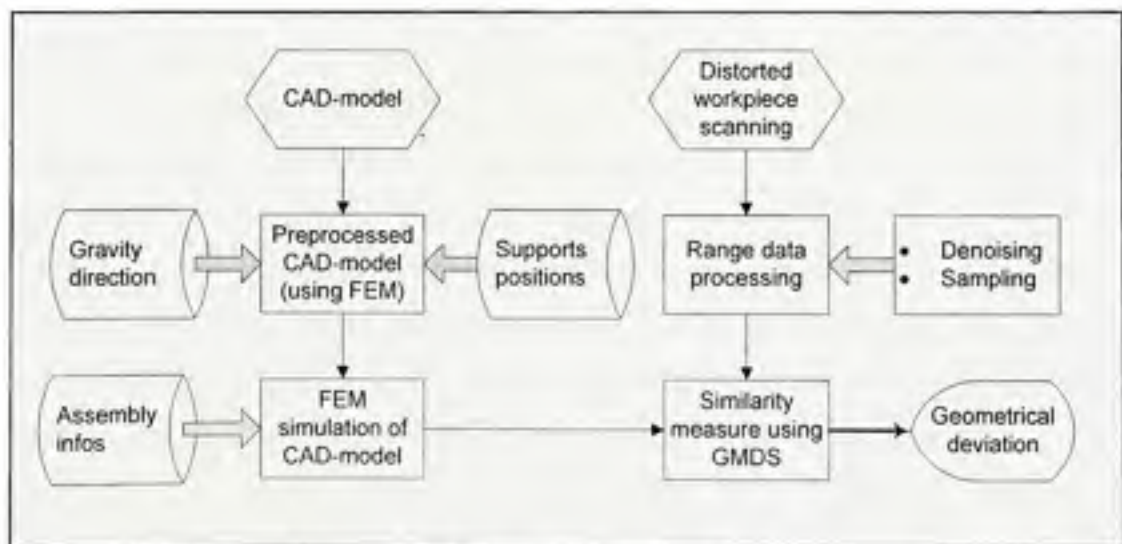


Figure 3.8 Inspection process flowchart.

Here we propose a second measuring methodology. Instead of using a free-shape CAD model as a virtual fixture and modeling the range data (used for FEM analysis), a point cloud of scanned data will be used as numerical fixture. With this method there is no need to resort to the exhausting and time-consuming modeling process of range data. Pre-processed measured data come together with a free-shape CAD-model. Note that the CAD-model should be previously analysed, applying the gravity effect at the same direction as the scanning process (Fig 3.8).

3.5 Generalized numerical inspection fixture

In a previous section we considered the assembly information as prior knowledge. Here we are going to try without this information. To this end, the part is set-up onto reference support points. As mentioned earlier, the position of these reference points are clearly defined within the part frame. The workpiece is scanned in a distorted state without a fixation device. Instead of using a free-shape CAD model as virtual fixture and modeling the range data (used for FEM analysis) as in Weckenmann and Gabbia (2005), point clouds of scanned data will be used as numerical inspection fixtures. In this way, there is no need for the time-consuming segmentation and modeling process of range data. Preprocessed measured data come together with a preprocessed CAD-model. Note that the CAD-model should be previously analyzed, applying the gravity and support effects in the same direction as the scanning process (Fig. 3.9). The transformations that map the preprocessed CAD-model towards range data can be obtained by regular ICP method. In practice and at this stage, we put the measuring part on the inspection fixture. In our methodology this range data plays the role of inspection fixture and we call it: Numerical inspection fixture. Note that the embedding process does not need primary surface registration, so the similarity detection can take place before the rigid registration. The contour can be used for mapping the preprocessed CAD-model into the range data. We call the mapping which is done by GMDS and FEM, Nonrigid finite element registration. Generalized multidimensional scaling can be used as isometry-invariant partial surface matching so there is no need for perfect contour

hypothesis as in Abenhaim, Tahan et al. (2009). Defects due to geometric deviation can be found after finite element nonrigid registration, eliminating the spring-back effect.

Also of note is that the meshed CAD-model and the scanned workpiece may have a different number of vertices. Finally, this is notable in that internal stress after the assembly process can be predicted with the proposed method.

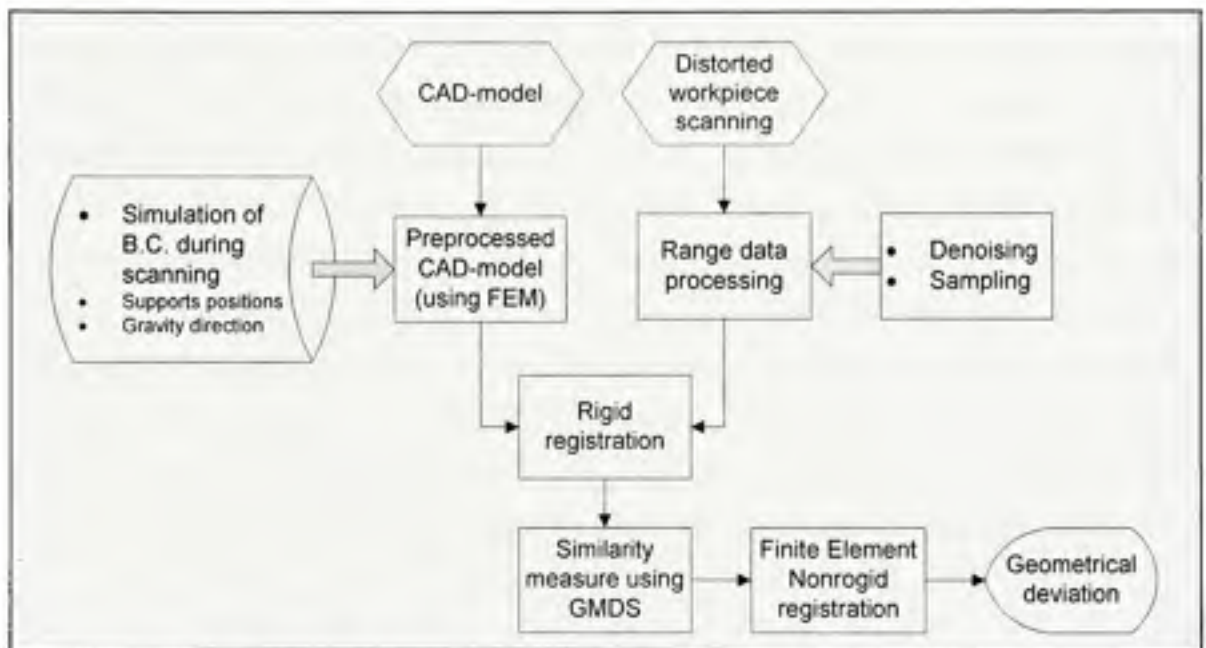


Figure 3.9 Inspection process flowchart using GNIF.

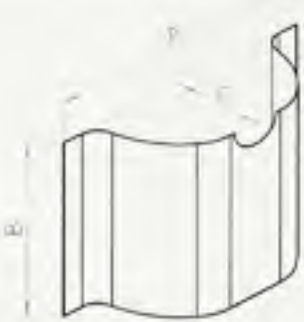
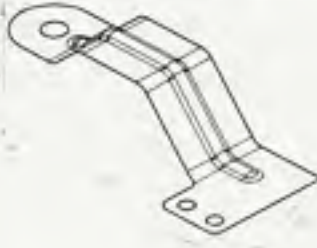

For large deformations, as the similarity measure only depends on surface intrinsic geometry, correspondence between the preprocessed CAD-model and range data is still calculable. In other words, similarity measure is independent from amount of deformation. This feature is notable especially in huge parts with large range of deformations. The workpiece can be scanned in a production line or it is indispensable for a fast scanning process. The other steps are realized using a PC. Thus, there is no more need to stop production lines for testing a workpiece.

CHAPTER 4

RESULTS

We have tested our methodology in a series of typical mechanical parts. This section presents three sample case studies that evaluate performance and validate the methods developed in previous sections. To this end, the free-form model is simulated by CATIA® and a finite element analysis of the model is done using ANSYS® and MATLAB®. Point clouds of free-form and free-state are simulated with a different number of vertices to evaluate the geodesic distance interpolation. On one hand, in order to better represent the underlying surface deviation, we prefer the point sampling to be as dense as possible. On the other hand, we need to keep in mind that the discrete representation is used by computer algorithms, and every additional point increases storage and computational complexity costs. To this end we have used *Voronoi tessellation* in order to represent the sampled discrete nodes of (metric) surface. Due to the fact that we have used the predefined deformation in range data generation step, qualitative performance evaluation is effectively traceable. We have divided our case studies in two categories for the parts belong to zone 'B' and 'C' (Figure 3.3). Overall, the size and engineering properties of three case studies is represented in Table 1.

Table 1 Overall size and engineering data.

| 1 st case study | 2 nd case study | 3 rd case study |
|---|--|---|
|  <p data-bbox="285 666 428 723">1400x1000x450 $t = 0.5$</p> |  <p data-bbox="706 628 821 675">330x130x47 $t = 0.1$</p> |  <p data-bbox="1178 599 1306 647">998x393x132 $t = 1$</p> <p data-bbox="1056 675 1342 780">Young's modulus = $2e+11$ Pa Poisson's ratio = 0.3 Density = 7850 kg/m³ All dimensions in mm.</p> |

4.1 Geometric inspection in absence of spring-back

In this section we assume that a part is set up on the *reference points* where the position is clearly defined within the part frame. Then, the part is scanned in a distorted manner without any fixation. A free-shape CAD model is processed applying gravity and other boundary conditions such as support positions, much like in the real measuring process. We assume that the workpiece belongs to the zone 'C' which means the part is flexible enough so that the spring-back effect is negligible. The similarity measure is calculated using GMDS. The primary nonrigid registration is done using the same reference points as in the setup procedure. Then the geometrical deviations are identified using the equation (3.1). We have tested this methodology with two mechanical parts shown in Fig. 4.1 and Fig. 4.2. Only the maximum geometric deviation is presented. The results are presented in Tables 2 and 3. For better visualization, a sampled tessellated section of the part is illustrated in Fig. 4.3. Geodesic distance interpolation enables us to accurately measure the similarity between CAD and scanned data. There is still no exact nodal correspondence.

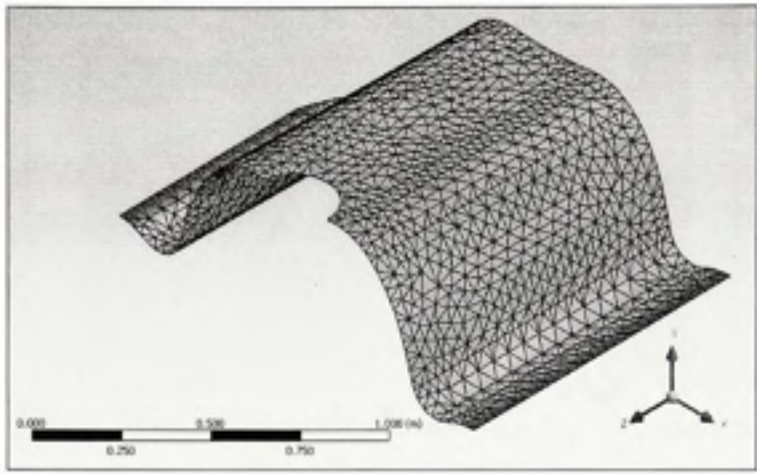


Figure 4.1 First case study.

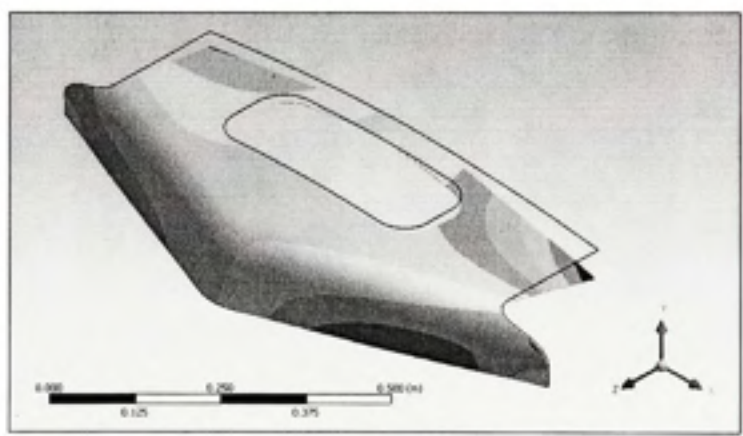


Figure 4.2 Second case study.

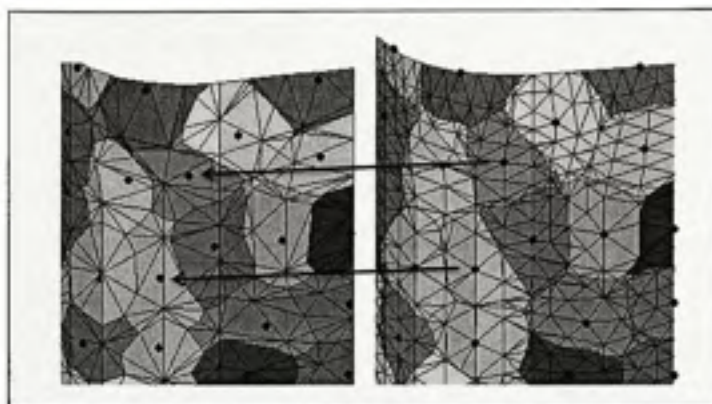


Figure 4.3 Similarity measure between the CAD models and range data.

**Table 2 Numerical fixture verification
(1st case study)**

| | Sampled points | $R_{max y}$ ($\times 10^{-2}$) [m] |
|---|---------------------------|---|
| Numerical inspection fixture | 50 | 1.16 |
| | 500 | 1.31 |
| Exact variation with ANSYS[®] | 5000 | 1.31275* |

*Considered as reference value

**Table 3 Numerical fixture verification
(2nd case study)**

| | Sampled points | $R_{max y}$ ($\times 10^{-2}$) [m] |
|---|---------------------------|---|
| Numerical inspection fixture | 50 | 1.03 |
| | 500 | 1.15 |
| | 1000 | 1.20 |
| Exact variation with ANSYS[®] | 5200 | 1.2333* |

*Considered as reference value

4.2 Inspection results with GNIF

The aim of this section is to generalize what we have done in previous sections. Furthermore, we consider the spring-back effect in the geometric inspection of flexible parts. To this end, the part is setup in reference points and scanned in distorted manner. The predefined spring-back was added to the same case studies as in previous sections. A more sophisticated one, such as Fig 4.4, was generated. The same methodology as in the section 3.5 was applied. The transformations that map the preprocessed CAD-model towards range data were obtained by a regular ICP method. A nonrigid finite element registration was applied finding the correspondence between the CAD-model and range data on both the contour areas. We remember that a GMDS is capable of isometry-invariant partial surface matching. This means that the contour matching can be safely done in the existence of deviation in the contour. The results are shown in Table 4. It should be mentioned that we have used a meshed CAD-model and range data with a different number of vertices. But for the process of computational speed both of them were sampled by Voronoi tessellation.

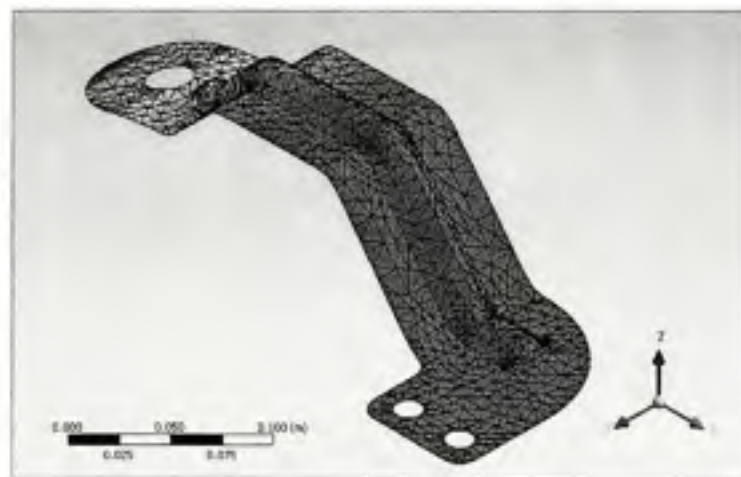


Figure 4.4 Third case study.

Table 4 GNIF verification

| | <i>1st case study</i> | <i>2nd case study</i> | <i>3rd case study</i> |
|--------------------------------------|----------------------------------|----------------------------------|----------------------------------|
| | $R_{max y} [m] (\times 10^{-2})$ | $R_{max y} [m] (\times 10^{-2})$ | $R_{max z} [m] (\times 10^{-1})$ |
| GNIF Results | 0.96 (548, 129)* | 0.89 (485, 139) | 0.91 (889, 93) |
| | 1.29 (1267, 218) | 1.29 (1359, 257) | 1.10 (1164, 170) |
| Maximum predefined deviation* | 1.3127 | 1.35 | 1.42 |

* The values between parentheses represent the part and contour sampled points respectively.

* Considered as reference value.

CONCLUSION

Including *part compliance with intrinsic geometry of surface* in metrology of free-form surfaces is an area of research pioneered in this paper. We merged the technologies in metric and computational geometry along with statistics and finite element methods to develop a general approach to the geometrical inspection of nonrigid parts. This method enables us to verify a diverse range of flexible parts without using special inspection fixtures. Although we have tried to present convincing results, no method with such promise is likely to be widely accepted until more practical testing can be done. Despite the fact that the proposed GNIF method is quite efficient, there is plenty of work to do for future computational speedup and accuracy. As a matter of fact, the proposed method is not a perfect and faultless substitution for inspection fixtures and CMM reports. However, in real-time applications it can be used for variational control of production lines so there will be no more need to stop production to test a workpiece.

Comparison of methods

As a matter of fact, little research has been done in the field of computer aided inspection comparing CAD/CAM, especially if the discussed field is nonrigid inspection. The witness claim is the amount of software in the competitive computer-aided market. Generally speaking, and as shown in the review of previous research, three distinguished research projects have been completed in the field of nonrigid inspection.

In spite of the work done at the University of Erlangen-Nürnberg by Weckenmann *et al.* (2005), our method does not need to transform the scanned data into a CAD-model. For parts with varying thickness their method is particularly useless. Assuming uniform thickness, the reverse engineering modeling of point clouds is a completely boring and time-consuming process.

The proposed method by Lartigue *et al.* (2006) at LURPA (Laboratoire universitaire de recherche en production automatisée / université de Paris) uses the same setup points as in the scanning process in rigid registration stages. Their proposed method does not consider spring-back effect. This is expected for really flexible materials (Zone 'C') but the problem is that the nature of SDT is not suitable for large deformations.

Iterative displacement inspection method, developed at the École de technologie supérieure (ÉTS) by Abenhaim *et al.* (2009) includes the vast limitations. Continuity (surface without holes, etc ...), thickness uniformity, and flawless boundaries are the essential prerequisites of this proposed method. The major flaw in this method is hidden in the fact that the method strongly depends on finding some trials and prior flexibility parameters which may vary according to thickness. The mentioned limitations cause the IDI to be inefficient in real engineering applications.

Limitations of GNIF

In the proposed inspection methodology, and for a full process automatization, we used the contour for nonrigid, isometry-invariant, surface matching. In fact, this is the only way to proceed when there is no prior knowledge of assembly joints and areas. This is not what to expect for a vast range of engineering applications. For more crucial results, prior information in assembly joints is needed. In production lines, and for each series of products, this information is available, in spite of what is proposed by Weckenmann and Gabbia (2005), full automatization of the inspection process is still available.

Contributions

The significant contributions made by this thesis include the following:

- 1) A comprehensive system was developed for the nonrigid geometric inspection of flexible parts. Bibliographical research shows that we are the first to include the intrinsic geometry of surface in the metrology of flexible parts.

- 2) Two methodologies for dealing with flexible material inspection were proposed, implemented and tested. The results were very promising.
- 3) Real engineering case studies including holes, radiuses, chamfers and sharp edges were performed. The parts, as well as range data, were meshed with different meshing strategies involving a different number of vertices. In this way, we were assured that there is no exact correspondence between the vertices in a CAD-model and range data. The then proposed methodologies were applied to these case studies.
- 4) Unlike the usual, we mapped the CAD-model into range data. As the mapping between the range data and CAD-model was bijective-distance-preserving, there was no more need to transform the point cloud into a computer aided analyzable model which is a very time-consuming process.
- 5) Large deformations are completely normal, especially for huge parts such as automobile and aircraft bodies. Where appropriate, large deformations were included into the case studies. Generalized numerical inspection fixtures were implemented and tested. The results were encouraging.
- 6) Unlike the methods presented by other authors using an embedding process, to find the similarity between a CAD-model and range data (two different metric spaces), there is no need for primary surface registration. This really speeds up the measuring process, especially when we have prior information about the assembly process.
- 7) One of the significant specifications of generalized numerical inspection fixtures were the capability for isometry-invariant partial surface matching. This means that contour matching can be safely utilized in the existence contour deviation.

- 8) It is of note that that the presented method is capable of predicting the produced stress during the assembly process. This stress can be considerable for large deformations and should be taken into account in some applications.
- 9) The presented method for the identification of geometric deviation enabled us to define a new interpretation for maximum geometric deviation.

RECOMMENDATIONS

A new method has been developed and presented for the geometric inspection of flexible parts using *generalized numerical inspection fixture*. Several topics that should be investigated further arose during the course of this research. The most promising of them are briefly described in this section. Future work in this area should expand and further verify the new method.

- 1) The GNIF method has been presented and verified in this paper using the case studies in real engineering applications. Future work should develop more accurate geodesic distance calculation in discrete *domains*, especially in the algorithm's update stage.
- 2) Although in this paper we used the intrinsic geometry of surfaces for similarity measures between discrete topologies, other methods like the *Coherent Point Drift* algorithm should be verified as similarity measures.
- 3) With modern technologies such as laser scanners, millions of points presenting the surface topology are accessible. This means that the simple Dijkstraalgorithm in graphs may give the closest results in comparison with the fast marching method. This is something that requires further research.
- 4) This work can be criticized because we dealt with noiseless data. It is evident that the noise will affect the proposed method. This effect, as well as the effect of the diverse smoothing methods, should be studied in depth.
- 5) Further deepening of this research would involve studying measuring uncertainty and classifying it with surface extrinsic geometry.
- 6) Actually, this study may be criticized relentlessly due to a lack of practical experiments. In spite of the fact that we tried to present persuasive results, especially for the second

methodology (GNIF), there is no equivalent method for comparison and accurate assessment. Future work should expand and verify our presented methods with practical tests.

- 7) Finally we note that the same numerical framework can be used for computing form geometrical tolerances (H.R.E and S.A.T., unpublished results).

ANNEX I

PUBLICATIONS

The publications created by this thesis include the following:

- 1) H. R. Esfahlan and S. A. Tahan, "Nonrigid geometric inspection using intrinsic geometry," in *Proceedings of the CSME forum 2010* Victoria, 2010.
- 2) H. R. Esfahlan, J. F. Chatelain and S. A. Tahan, "Nonrigid geometric metrology using generalized numerical inspection fixture," *Precision Engineering*, 2010, "*Unpublished*".

ANNEX II

SMACOF algorithm

```
%% Demonstration of multidimensional scaling using SMACOF
algorithm
load lst_case_study

% embedding using SMACOF
X0 = [surface_x.X,surface_x.Y,surface_x.Z];
[X_smacof,hist_smacof] = smacof(surface_x.D,X0);

% shows the results at each iteration
for k = 1:length(hist_smacof.time),

trisurf(surface_x.TRIV,hist_smacof.X{k}(:,1),hist_smacof.X{k}(
:,2),hist_smacof.X{k}(:,3));
    axis image; shading flat; lighting phong; camlight head;
    pause(0.1);
end

%% SMACOF algorithm
function [X,hist] = smacof(D,X0)
iter = 20; % number of iterations in SMACOF method

% initialize
iii = 1;
Z = X0;
X = X0;
D_ = squareform(pdist(X,'euclidean'));

% initialize history
hist.s(1) = calc_stress(X0,D);
hist.X{1} = X0;

fprintf(1,'iter          stress   time (sec)\n')
fprintf(1,'INIT      %12.3g   -----\n', hist.s(1))

while (iii <= iter),
    t = cputime;

    B_ = calc_B(D_,D);
    X_ = B_*Z/size(D,1);
    D_ = squareform(pdist(X,'euclidean'));
```

```

S = calc_S (D,D_);
Z = X;

% add history
    hist.time(iii) = cputime-t;
    hist.s(iii) = calc_stress(X,D);
    hist.X{iii} = X;

        fprintf(1,'%4d  %12.3g  %10.3g\n',
iii,hist.s(iii),hist.time(iii))

    iii = iii+1;

end

%% Sub-functions

% compute the stress
function [S] = calc_stress (X,D)
D_ = squareform(pdist(X,'euclidean'));
S = calc_S (D,D_);
return

function [S] = calc_S (D,D_)
d = triu((D - D_).^2,1);
S = sum(d(:));
return

function [B] = calc_B (D_,D)
B = zeros(size(D));
i = find(D_(:) ~= 0);
B(i) = - D(i)./D_(i);
B = B - diag(diag(B));
d = sum(B);
B = B - diag(d);
return

```

ANNEX III

Hausdorff distance algorithm

We have submitted the following code into MATLAB's *File Exchange* toolbars. The algorithm computes the Hausdorff distance between two point clouds and is accessible at the following address:

<http://www.mathworks.com/matlabcentral/fileexchange/27905-hausdorff-distance>

```
%% Hausdorff Distance: Compute the Hausdorff distance between
two point clouds.
% Let A and B be subsets of a metric space (Z,dZ),
% The Hausdorff distance between A and B, denoted by dH (A,
B), is defined by:
% dH (A, B) = max{sup dz(a,B), sup dz(b,A)}, for all a in A, b
in B,
% dH(A, B) = max(h(A, B),h(B, A)),
% where h(A, B) = max(min(d(a, b))),
% and d(a, b) is a L2 norm.
% dist_H = hausdorff( A, B )
% A: First point sets.
% B: Second point sets.
% ** A and B may have different number of rows, but must have
the same number of columns. **
%

function [dist] = hausdorff(A, B)
if(size(A,2) ~= size(B,2))
    fprintf( 'WARNING: dimensionality must be the same\n' );
    dist = [];
    return;
end
dH = max(compute_dist(A, B), compute_dist(B, A))
```

```
%% Compute distance
function[dist] = compute_dist(A, B)
m = size(A, 1);
n = size(B, 1);
dim= size(A, 2);
for k = 1:m
    C = ones(n, 1) * A(k, :);
    D = (C-B) .* (C-B);
    D = sqrt(D * ones(dim,1));
    dist(k) = min(D);
end
dist = max(dist);
```

ANNEX IV

GLOSSARY

Bijection a map that is *surjective* and *injective*. Bijective maps have an inverse.

Free shape corresponds to CAD-model in absence of gravity and assembly constraints.

Free-state variation is a term used to describe distortion of a part after removal of forces applied during manufacture.

Geodesic is a locally length-minimizing curve.

Hausdorff space a *topological space* (X, T) , in which for every distinct x, y , there exist disjoint open sets $U, V \in T$ such that $x \in U$ and $y \in V$.

Injection (one-to-one map) a map $f: X \rightarrow Y$ associating distinct argument to distinct values, such that $f(x_1) = f(x_2)$ implies $x_1 = x_2$ for all $x_1, x_2 \in X$.

Intrinsic geometry generic name for properties of a Riemannian manifold, expressible in terms of the distance structure.

Isometric embedding a distance-preserving map.

Isometry *bijective* distance-preserving map.

Metric space (denoted by (X, d_X)) a space X equipped with a *metric* d_X .

Nonrigid finite element registration is the mapping of CAD-model into range data which is done by GMDS and FEM.

Surjection (onto map) a map $f: X \rightarrow Y$, whose range spans the whole codomain, i.e., $f(X) = Y$.

Symmetric matrix a square matrix A satisfying $A^T = A$.

Topological space denoted by (X, T) is a space X equipped with a *topology* T .

REFERENCES

- Abenheim, G., S. Tahan, et al. (2009). A novel approach for the inspection of flexible parts without the use of special fixtures , "*Unpublished*".
- Aleksandrov, A. and V. Zalgaller (1967). *Intrinsic geometry of surfaces*, American Mathematical Society.
- Amberg, B., S. Romdhani, et al. (2007). "Optimal step nonrigid ICP algorithms for surface registration." 1-8.
- Bentley, J. (1975). "Multidimensional binary search trees used for associative searching." *Communications of the ACM* **18**(9): 517.
- Besl, P. and H. McKay (1992). "A method for registration of 3-D shapes." *IEEE Transactions on pattern analysis and machine intelligence* **14**(2): 239-256.
- Bourdet, P. and A. Clément (1976). "Controlling a complex surface with a 3 axis measuring machine." *Annals of the CIRP* **25**(1): 359-361.
- Boyd, S. and L. Vandenberghe (2004). *Convex optimization*, Cambridge Univ Pr.
- Bronstein, A., M. Bronstein, et al. (2007). *Numerical geometry of non-rigid shapes*, Springer-Verlag New York Inc.
- Bronstein, A., M. Bronstein, et al. (2006). "Generalized multidimensional scaling: a framework for isometry-invariant partial surface matching." *Proceedings of the National Academy of Sciences* **103**(5): 1168.
- Bronstein, A., M. Bronstein, et al. (2007). "Efficient computation of isometry-invariant distances between surfaces." *SIAM Journal on Scientific Computing* **28**(5): 1812-1836.
- Burago, D., Y. Burago, et al. (2001). *A course in metric geometry*, American Mathematical Society Providence, RI.
- Chang, M. and D. Gossard (1997). "Modeling the assembly of compliant, non-ideal parts." *Computer-aided design* **29**(10): 701-708.
- Cox, M. (2000). *Multidimensional scaling*, CRC Press.
- Creveling, C. (1997). *Tolerance design: a handbook for developing optimal specifications*, Addison-Wesley, Reading, Mass.

- Dahlström, S. and L. Lindkvist (2007). "Variation simulation of sheet metal assemblies using the method of influence coefficients with contact modeling." *Journal of manufacturing science and engineering* **129**: 615.
- Dijkstra, E. (1959). "A note on two problems in connexion with graphs." *Numerische mathematik* **1**(1): 269-271.
- Elbaz, A. and R. Kimmel (2003). "On bending invariant signatures for surfaces." *IEEE Transactions on pattern analysis and machine intelligence* **25**(10): 1285-1295.
- Greenspan, M. and G. Godin (2001). A nearest neighbor method for efficient ICP. *Proc. of the 3rd Int. Conf. on 3-D Digital Imaging and Modeling (3DIM01)*.
- Kimmel, R. and J. Sethian (1998). "Computing geodesic paths on manifolds." *Proc. Natl. Acad. Sci. USA* **95**(15): 8431-8435.
- Lartigue, C., F. Thiebaut, et al. (2006). Dimensional metrology of flexible parts: Identification of geometrical deviations from optical measurements. *Advanced mathematical & computational tools in metrology VII*: 196.
- Levy, B. (1984). "Empirically derived equations for predicting springback in bending." *Journal of Applied Metalworking* **3**(2): 135-141.
- Li, K., W. Carden, et al. (2002). "Simulation of springback." *International Journal of Mechanical Sciences* **44**(1): 103-122.
- Liu, S. and S. Hu (1997). "Variation simulation for deformable sheet metal assemblies using finite element methods." *Journal of manufacturing science and engineering* **119**: 368.
- Mémoli, F. and G. Sapiro (2005). "A theoretical and computational framework for isometry invariant recognition of point cloud data." *Foundations of Computational Mathematics* **5**(3): 313-347.
- Myronenko, A., X. Song, et al. (2007). "Non-rigid point set registration: Coherent Point Drift." *Advances in Neural Information Processing Systems* **19**: 1009.
- Peyré, G. and L. Cohen (2006). "Geodesic remeshing using front propagation." *International Journal of Computer Vision* **69**(1): 145-156.
- Rouy, E. and A. Tourin (1992). "A viscosity solutions approach to shape-from-shading." *SIAM Journal on Numerical Analysis*: 867-884.
- Rusinkiewicz, S. and M. Levoy (2001). "Efficient variants of the ICP algorithm." 145-152.

- Schwartz, E., A. Shaw, et al. (1989). "A numerical solution to the generalized mapmaker's problem: flattening nonconvex polyhedral surfaces." *IEEE Transactions on pattern analysis and machine intelligence* **11**(9): 1005-1008.
- Sethian, J. (1996). "A fast marching level set method for monotonically advancing fronts." *Proceedings of the National Academy of Sciences* **93**(4): 1591.
- Sethian, J. (1999). *Level set methods and fast marching methods*, Cambridge university press Cambridge.
- Sethian, J. (2008). "Theory, algorithms, and applications of level set methods for propagating interfaces." *Acta numerica* **5**: 309-395.
- Standard, A. (1994). "Dimensioning and Tolerancing, ASME Y14. 5M-1994." American Society of Mechanical Engineers, New York.
- Tsitsiklis, J. (1995). "Efficient algorithms for globally optimal trajectories." *IEEE Transactions on Automatic Control* **40**(9): 1528-1538.
- Weckenmann, A. and A. Gabbia (2005). *Testing formed sheet metal part using fringe projection and evaluation by virtual distortion compensation. The 5th International Workshop on Automatic Processing of Fringe Patterns*, Springer.